Master's thesis

NTNU
Norwegian University of Science and Technology
Faculty of Information Technology and Electrical Engineering
Department of Electronic Systems

Erik Buer

Characterization of Modulated Chirp Signals

Master's thesis in Electronic Systems Design
Supervisor: Stefan Werner
June 2020

NTNU
Norwegian University of Science and Technology

KONGSBERG

Erik Buer

Characterization of Modulated Chirp Signals

Master's thesis in Electronic Systems Design
Supervisor: Stefan Werner
June 2020

Norwegian University of Science and Technology
Faculty of Information Technology and Electrical Engineering
Department of Electronic Systems

NTNU
Norwegian University of
Science and Technology

Abstract

This thesis is a master's dissertation concluding a master of science in signal processing and communications. It studies the estimation of center frequency, Instantaneous Frequency (IF) and the symbol rate of *chirp-per-symbol* Spread Spectrum (SS) communication signals. Parameter estimators are implemented and their performance is measured against non-linear and discontinuous chirp modulated signals.

A center frequency estimator based on cycle-frequency correlation and a symbol rate estimator based on harmonic cycle-frequencies is proposed and compared to traditional methods. Various traditional and modern IF estimators are compared and studied on various chirp signals.

Statistical analysis shows that a center frequency estimate can be assembled based on the spectral correlation at specific cycle-frequencies, obtaining accuracies that approach that of a second-order interpolated magnitude spectrum Maximum Likelihood Estimation (MLE) method. From this, it is apparent that estimates of the center frequencies can be obtained for multiple signals overlapping in time and frequency by studying their cycle-frequencies.

For IF estimation a piece-wise polynomial IF estimator is shown to outperform all of the studied estimators on discontinuous chirps. It suffers from high computing requirements, but is exceptionally parallelizable. Faster Time-Frequency (TF) based estimators are studied. Of these the Hilbert-Huang Transform (HHT) is shown to outperform the Wigner-Ville Distribution (WVD) for use with MLE of discontinuous chirps in moderate Signal-to-Noise Ratio (SNR).

The symbol rate of a chirp signal is found to be estimated computationally efficiently through a harmonic cycle-frequency Maximum Likelihood (ML) estimate. In two out of three studied cases, this estimator outperforms an autocorrelation-based counterpart, both in execution time and accuracy.

Sammendrag

Denne avhandlingen er en masteroppgave som konkluderer en "master of science" i signalbehandling og kommunikasjon. I oppgaven studeres estimering av senterfrekvens, instantan frekvens og symbolhastigheten til frekvensrampe *spredd spektrum* kommunikasjonssignaler. Det er utviklet signalgeneratorer og parameterestimatorer. Ytelsen til estimatorene er målt mot de genererte ikke-lineære og ikke-kontinuerlige frekvensrampemodulerte signaler.

En syklusfrekvens-basert senterfrekvensestimator og en symbolhastighetsestimator basert på harmoniske syklusfrekvenser er utviklet, og sammenlignet med tradisjonelle metoder. Ulike tradisjonelle og moderne instantan frekvensestimatorer er sammenlignet og studert på forskjellige frekvensrampesignaler.

Ved bruk av statistisk analyse er det vist at et senterfrekvensestimat kan dannes basert på spektral korrelasjon ved spesifikke syklusfrekvenser, og oppnå en nøyaktighet oppimot det en andreordens interpolert magnitudespektrum sannsynlighetsmaksimerende metode har. Det vil si at estimater av senterfrekvens kan oppnås for flere signaler som overlapper i tid og frekvens, ved å studere deres syklusfrekvenser.

For estimering av instantan frekvens er det vist at en stykkevis polynom-basert estimator oppnår høyest nøyaktighet av de studerte estimatorene på ikke-kontinuerlige frekvensramper. Den lider av høy utregningstid, men er i stor grad parallelliserbar. Raskere tid-frekvens baserte estimatorer er undersøkt. Av disse utkonkurrerer Hilbert-Huang-transformen, Wigner-Ville for bruk med sannsynlighetsmaksimerende estimater av ikke-kontinuerlige frekvensrampesignaler i moderat signal-til-støyforhold.

Det er vist at symbolhastigheten til et frekvensrampesignal kan beregnes tidseffektivt gjennom et harmonisk syklusfrekvensestimat. I to av tre undersøkte tilfeller er denne metoden bedre enn en autokorrelasjonsbasert metode både på utregningshastighet, og nøyaktighet.

Acknowledgement

I would like to thank my supervisors Erik Narverud and Stefan Werner for motivation and guidance throughout this project. I would also like to thank Kongsberg Defence & Aerospace AS for allowing me to work on their behalf. Lastly, i would like to thank my girlfriend Ida Marie, for supporting me through this semester.

Contents

Acronyms

ADC Analog-to-Digital Converter. 1

BFGS Broyden-Fletcher-Goldfarb-Shanno. 24
BW bandwidth. 26, 27, 41

CAF Cyclic Autocorrelation Funcion. 19
CRLB Cramer-Rao Lower Bound. 17
CS Cyclostationary. 3, 18, 19, 25–27, 34, 37, 38, 40, 41
CSS Chirp Spread Spectrum. 2
CWD Choi-Williams Distribution. 42

DFT Discrete Fouriere Transform. vii, 10–12, 21, 22, 26, 34, 40
DSP Digital Signal Processing. 2, 4
DWD Discrete Wigner Distribution. 15

ECM Electronic Countermeasures. 1
EMD Empirical Mode Decomposition. 15
ESM Electronic Support Measures. 2

FAM FFT Accumulation Method. 19, 25, 40
FFT Fast Fourier Transform. 11, 19, 21
FIR Finite Impulse Response. 13, 21, 24, 30
FPGA Field-Programmable Gate Array. 40

GMM Gaussian Mixture Model. 10, 25
GPU Graphics Processing Unit. 40

HHT Hilbert-Huang Transform. i, 13, 15, 24, 30, 32, 33, 40, 43
HOC Higher Order Cumulant. 3
HOM Higher Order Moment. 18

IC Integrated Circuit. 40
IDFT Inverse Discrete Fouriere Transform. 6
IF Instantaneous Frequency. i, 2–6, 8, 12, 13, 15–18, 23–25, 30–33, 39–43
IMF Intrinsic Mode Function. 15, 16, 33, 40

LFM Linear Frequency Modulation. 6, 7, 17, 24, 28, 29, 31–33, 36–38, 40–42
LoRa Long Range (proprietary physical layer standard). 3, 8, 9, 13, 14, 17, 23, 41, 43

MAE Mean Absolute Error. 10, 30, 34
MIMO Multiple-Input and Multiple-Output. 6, 41
ML Maximum Likelihood. i, 11, 18, 20, 24, 32, 35, 40, 42, 43
MLE Maximum Likelihood Estimation. i, 1, 10, 12, 15, 17, 18, 24, 26, 27, 30–35, 39
MR Modulation Recognition. 1, 18

NLFM Non-Linear Frequency Modulation. 5–8, 15–19, 21, 24, 28–31, 33–37, 39–43

PD Probability of Detection. 1
PDF Probability Density Function. 25
PI Probability of Identification. 1
PSD Power Spectral Density. 6, 12, 19, 26, 29, 30, 40, 41
PSK Phase Shift Keying. 8
PWD Pseudo Wigner Distribution. 15, 42

QAM Quadrature Amplitude Modulation. 8
QIFT Quadratically-Interpolated FFT. 11

RF Radio Frequency. 1

SCD Spectral Correlation Density. 19, 25, 26, 35, 36, 40
SEI Specific Emitter Identification. 1, 17
SNR Signal-to-Noise Ratio. i, 2, 3, 8–10, 15, 17, 18, 30, 40, 41, 43
SS Spread Spectrum. i, 1, 2
STFT Short-Time Fourier Transform. 19, 40
SVM Support Vector Machine. 3

TF Time-Frequency. i, 3, 5, 7, 10, 13, 24, 40, 42

WGN White Gaussian Noise. 9, 11, 19
WSS Wide Sense Stationary. 19, 25
WVD Wigner-Ville Distribution. i, iv, 13–15, 17, 24, 30–33, 39, 42, 43

Notation and Definitions

a	is a scalar.
$\boldsymbol{a}$	is a vector.
$a[i]$	is a time series equivalent of $\boldsymbol{a}$. Zero-indexed.
$\boldsymbol{A}$	is a matrix.
$\mathbb{1}$	is a column vector of ones. Length defined by context: $\mathbb{1} = [1, 1, \ldots, 1]^T$.
$\hat{a}$	is an estimate of, or estimator for parameter a.
$\tilde{a}$	is a complex scalar $\mathrm{Re}\{\tilde{a}\} + i\,\mathrm{Im}\{\tilde{a}\}$.
$\tilde{a}^*$	is the complex conjugate of a scalar $\mathrm{Re}\{\tilde{a}\} - i\,\mathrm{Im}\{\tilde{a}\}$.
$\check{\boldsymbol{a}}$	is the Hilbert transformed vector $\boldsymbol{a}$.
$\mathcal{F}\{\cdot\}$	is the Discrete Fouriere Transform operator.
$\mathcal{Z}\{\cdot\}$	is the Z-transform operator.
$\mathbb{E}\{\cdot\}$	is the expectation operator.
$\mathcal{E}\{\cdot\}$	is the signal energy operator.
$\mathrm{mod}\,\cdot$	is the modulo operator.
$\arg\cdot$	is the argument (angle) operator.
$\lvert\cdot\rvert$	is the element-wise absolute value.
$\lVert\cdot\rVert$	is the norm of a vector.
$\langle a(x), b(x)\rangle$	is the inner product of $a(x)$ and $b(x)$.
$\langle a(x)\rangle_b$	is the average of $a(x)$ over b. Defined as $\langle a(x)\rangle_b \coloneqq \frac{1}{b}\int_{-b/2}^{b/2} a(x)\,\mathrm{d}x$.
$\lfloor a \rfloor$	is the greatest integer not superseding a, $a \in \mathbb{R}$.
R_{ab}	is the correlation of $\boldsymbol{a}$ and $\boldsymbol{b}$.
$\circledast$	is the convolution operator.
$\cdot$	is the dot-product operator.
$\times$	is the multiplication operator.
$[a..b]$	is the interval of integers $\mathbb{Z}$ from a to, and including b. $[a..b] = \left\{x \in \mathbb{Z} \middle\vert\, a \le x \le b\right\}$.
$[a, b]$	is the interval of real numbers $\mathbb{R}$ from a to, and including b. $[a, b] = \left\{x \in \mathbb{R} \middle\vert\, a \le x \le b\right\}$.
$\langle a, b\rangle$	is the interval of real numbers $\mathbb{R}$ between, but not including a or b. $\langle a, b\rangle = \left\{x \in \mathbb{R} \middle\vert\, a < x < b\right\}$.
$a \coloneqq b$	specifies that a is defined as b.

Vectors and matrices are one-indexed.
Time series are zero-indexed.
Vectors are unless otherwise noted column vectors.

Chapter 1

Introduction

1.1 Background and Motivation

In the defense and security sector, situational awareness is key. This includes knowing the numbers, positions, and types of adversaries. One way of obtaining such knowledge is through the radio spectrum. Modern surveillance systems utilize passive Radio Frequency (RF) receivers looking to detect, classify and position RF emitters. This classification can be divided into two objectives. Modulation Recognition (MR) which classifies the type (class) of modulation [1], and Specific Emitter Identification (SEI) which looks beyond the modulation and analyze specific traits in the signal, so-called fingerprints, in order to classify not only the class of modulation (e.g., communications standard) but the specific radio class, or even specific unit of a transmitter (e.g., a specific vehicle) [2]. This information can be used for situational awareness, or to efficiently counter the adversary with so-called Electronic Countermeasures (ECM).

State-of-the-art classification systems use a method that can be divided into three steps. First the system scans the spectrum for emissions e.g., though white space detection [3]. Then detected signals are separated and studied through banks of parameter estimators to create what is called a *feature vector*. This vector contains details about the observed signal. The vector is then fed into a classifier that outputs a class, like type of modulation, platform, etc. This method is called the *feature based* method*. An overview of the three steps is illustrated in Figure 1.1.

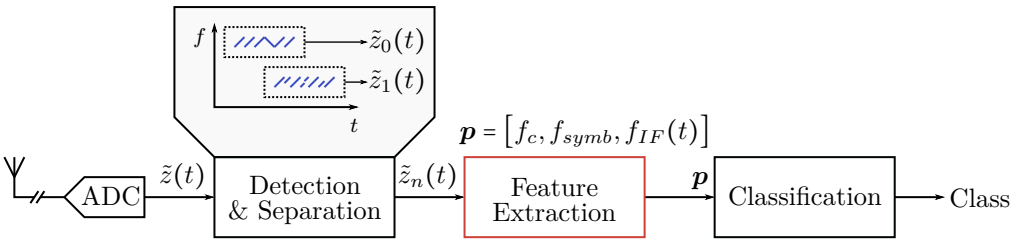

Figure 1.1: Three-Step Classification System (Thesis Focus in Red)

To reduce the Probability of Detection (PD) and Probability of Identification (PI) of radio signals, various techniques are used. Perhaps the most common technique is SS [5], where the spectral power density of a signal is reduced by spreading the payload signal over a wide bandwidth. This reduces the peak power envelope close to and below the background noise level, or "noise floor". This makes detection and identification challenging.

*A second class of methods is the MLE methods, which can be studied further in [4].

One SS method is the Chirp Spread Spectrum (CSS). In CSS the signal is spread in frequency by applying a frequency chirp to each symbol or packet. Traditionally linear chirps have been used, but state-of-the-art software-defined radios allow the use of more complex non-linear chirp signals [6]. Chirp signals can obtain large processing gains. By sweeping a wide bandwidth the signal obtains high resistance to narrow-band interference [7]. The large processing gains also enable low-power transmission and thus a low spectral power density. This wideband, low-power, low noise-density characteristic makes chirps challenging to detect, and classify. The close to infinite possible chirp IF trajectories require powerful and agile algorithms to characterize them.

There is a great deal of research on the detection and classification of traditional modulations [1]. However, less focus is put on chirp signals[†]. The goal is to develop a set of estimators which together can characterize most types of chirp modulations optimally in low SNR.

1.2 Problem Definition

Signal detection and classification as part of Electronic Support Measures (ESM) is widely adopted in the defense sector. Passive radio detectors are used to detect, classify, and position distant objects for increased situational awareness among other uses. Frequency modulated or chirp spread spectrum signals are widely used in radar and communication systems. An emerging technique is the use of nonlinear frequency modulated (NLFM) pulses. This brings the need for algorithms that can characterize these waveforms. The task is to develop an algorithm able to characterize chirp modulated communication signals. The resulting parameters are intended to be used in signal classification.

In this project the student will:

1. Develop a signal generator capable of generating various chirp modulated communication signals.
2. Develop an algorithm capable of characterizing chirp signals, and measure its performance.

1.3 Scenario and Focus

This thesis is based on the scenario of an intercept receiver searching for adversary emitters. An interceptor will want to intercept communications at short ranges and ranges superseding that of the target link. It will therefore observe signals of interest in a wide SNR range.

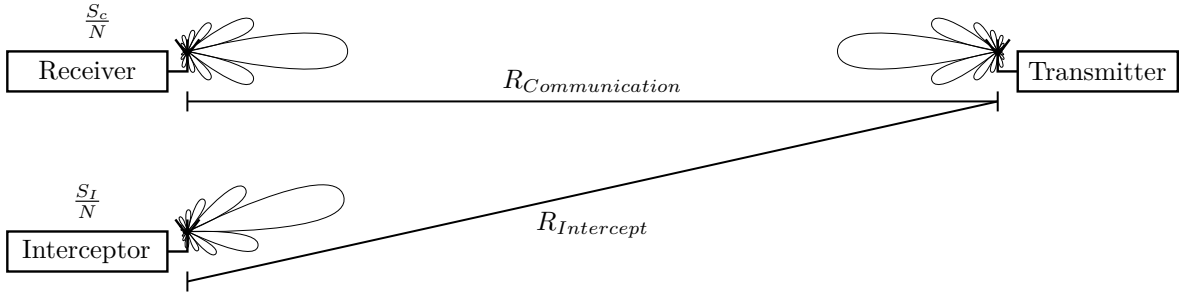

Figure 1.2: Intercept Scenario (Adapted From [8])

The receiver is utilizing digital sampling of a wide bandwidth, and Digital Signal Processing (DSP) for detection and classification (parameter estimation herein). An emission is detected and extracted as a time series. The receiver is assumed to have separated all simultaneous emissions to separate bins, such that only a single emission, packet or pulse train is present in each time series. This time series is transferred to a feature extractor which populates a feature vector with estimated parameters, and

[†]Outside of the radar community.

hands it off to a classification algorithm, e.g., a Support Vector Machine (SVM) [9]. This thesis takes on the estimation of particular features of chirp modulated signals. The algorithm specified in section 1.2 is implemented as a set of estimators. It is assumed that some prior signal sorting[‡] is performed such that the signal at this particular processing stage is known to be a chirp modulated signal.

The focus of this thesis is to study parameters that can be compared to a theoretical *true* value. The chosen parameters are center frequency, IF, and symbol rate. They are assumed by the author to provide a good decision distance between various chirp signals. Cyclostationary analysis is an emerging technique which shows promise [11], and is therefore used to assemble estimators. Multiple estimators are compared for each parameter in order to map their strengths and weaknesses. Two chirp classes with different challenges are used in order to highlight weaknesses in the estimators. The signal classes are continuous non-linear, and discontinuous linear chirps.

1.4 Organization

This thesis is organized into six chapters, where this is the first. The second chapter presents the theory of chirp signals, a method of generating non-linear chirps with "favorable" characteristics, and the basic structure of Long Range (proprietary physical layer standard) (LoRa) signals. Then a set of estimators including maximum likelihood center frequency estimator and several IF estimators utilizing various TF transforms are presented. Some intermediate results are presented to highlight estimator weaknesses which are widely known. Lastly, cyclostationary analysis and a traditional autocorrelation harmonic frequency estimator is presented.

The third chapter deals with the implementation of the generation and estimation algorithms. A method of generating linear and non-linear chirps, and the method used for assembling the estimators are presented. The methods of assembling IF estimators are presented together with a description of how their performance is measured. Then a cycle-frequency-based center frequency estimator is presented along with a procedure of how to utilize *a priori* knowledge with it. Lastly, a harmonic cycle-frequency estimator is presented as a symbol rate estimator, along with methods of utilizing *a priori* knowledge with it.

The fourth chapter presents various characteristics of the generated signals and the implemented estimators. The estimator performance is presented in the form of their error statistics in different Signal-to-Noise Ratio levels. IF estimator weaknesses are highlighted with additional non-statistical analysis of single estimate results. Some intermediate results are presented for the Cyclostationary estimators to highlight the characteristics of the applied signals, in addition to statistical performance as with the others.

In the fifth chapter, the strengths and weaknesses of the estimators are discussed. Some extrapolation on the performance of the estimators to their big picture consequences and possibilities are presented. Lastly, in the sixth chapter, the thesis is summarized.

[‡]An initial sorting can be achieved through simple fast estimators based on e.g., Higher Order Cumulants (HOCs) in a decision tree [10].

Chapter 2

Theory

In this chapter the core theoretical concepts are presented. It starts off with a presentation the fundamentals, and properties of the target signals. Thereafter the theory of relevant estimators and related DSP methods are presented.

2.1 Chirp Signals

A chirp is a complex exponential whose phase $\Phi(t)$ changes *non-linearly* as a function of time. A chirp is defined as [12]

$$\tilde{s}(t) \coloneqq a(t)e^{i\Phi(t)}, \tag{2.1}$$

where a is a real valued magnitude term, $t \in \mathcal{T} = [-\frac{T}{2}, \frac{T}{2}\rangle$ and T is the chirp period. When a is a scalar (constant), then the signal has a *constant envelope*. This is assumed from here on. The frequency of the signal at time instance t is the *instantaneous frequency* $\omega(t)$. It is defined as

$$\omega(t) \coloneqq \frac{\mathrm{d}\Phi(t)}{\mathrm{d}t}\,[\mathrm{rad}], \tag{2.2}$$

where the IF in Hertz is

$$f \coloneqq \frac{\omega}{2\pi}\,[\mathrm{Hz}]. \tag{2.3}$$

The "chirp bandwidth" is defined as

$$\Omega \coloneqq \int_{\mathcal{T}} \omega(t)\,\mathrm{d}t. \tag{2.4}$$

The rate of IF change, defined as the *chirp rate* is

$$\gamma(t) \coloneqq \tfrac{\mathrm{d}\omega(t)}{\mathrm{d}t}. \tag{2.5}$$

For linear chirps, the chirp rate is a scalar.

The following definitions are used throughout this thesis:
Single tone chirps are the set of signals which can be constructed by a single complex exponential. It has a single IF at any time instance. This is assumed from here on.
Continuous chirps are the set of chirps whose IF is continuous. The IF is continuous when Equation 2.6 holds*. Let ω be a function of the chirp IF.

$$\lim_{t\to c} \omega(c) = \omega(t), \qquad\qquad t \in \mathcal{T}. \tag{2.6}$$

*This definition holds for interior points of $\omega(t)$ only.

In the case of communication signals, the definition of continuity only applies throughout the symbol period $t \in \mathcal{T}$.
Linear chirps are chirps whose IF is a linear function of time.

$$\omega(t) = a_0 + a_1 t, \qquad t \in \mathcal{T},\ \boldsymbol{a} \in \mathbb{R}^2 \tag{2.7}$$

An example of a continuous linear chirp is displayed in Figure 2.1.
Non-linear chirps are chirps whose IF is a nonlinear (any) function of time.

$$\omega(t) = f(t), \qquad t \in \mathcal{T} \tag{2.8}$$

where f is any *real* function. An example of a continuous linear chirp is displayed in Figure 2.5.
Piece-wise linear chirps are chirps built of segments of linear chirps that have instantaneous changes in chirp rate, and/or IF in their intersection. These are considered a subset of Non-Linear Frequency Modulation (NLFM) chirps. Figure 2.1 through 2.3 display a *continuous, linear* chirp in the time-domain, TF domain, and frequency domain respectively.

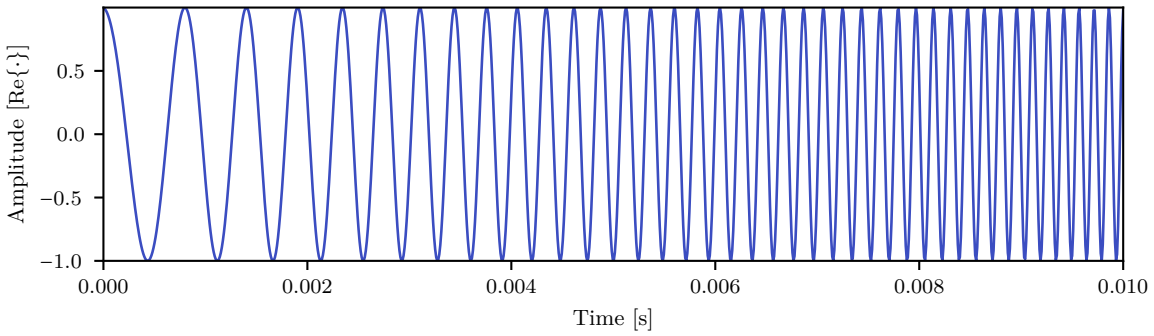

Figure 2.1: Constant Envelope Linear Chirp in the time domain, $s(t)$

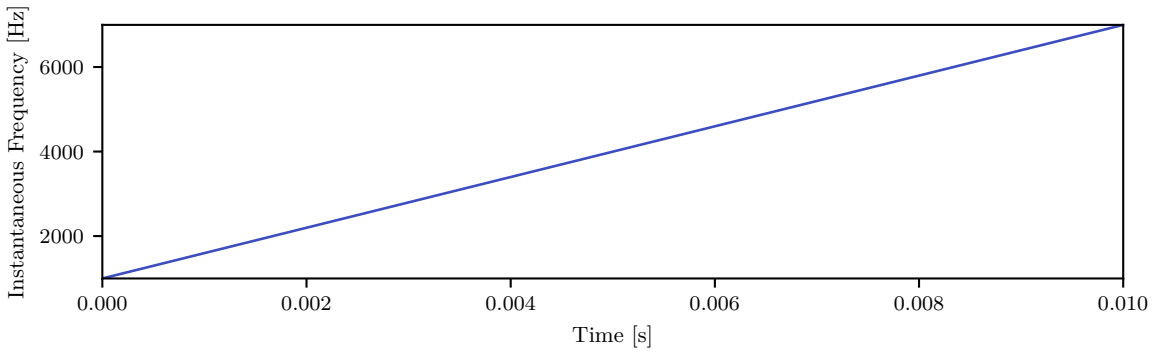

Figure 2.2: Angular Frequency $\omega(t)$ [Hz]

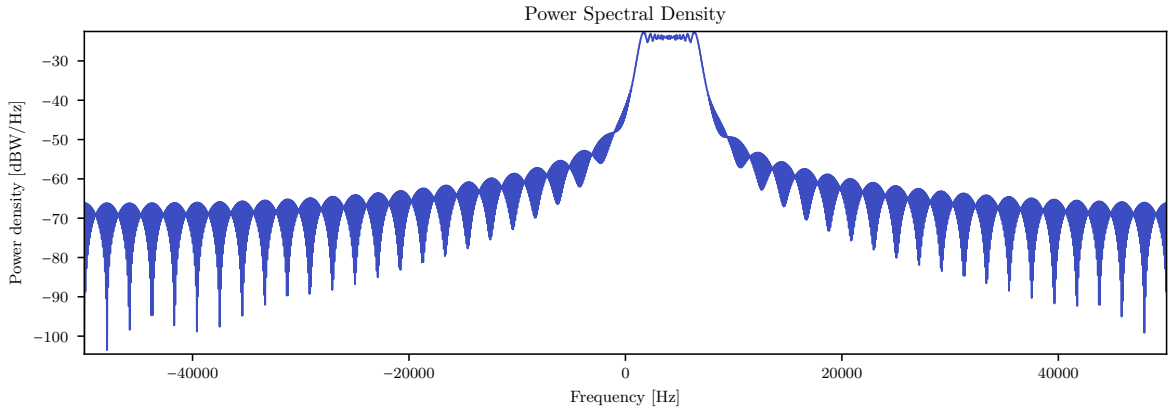

Figure 2.3: Linear Frequency Modulation (LFM) Periodogram

NLFM chirps have great flexibility in shape and characteristics. The IF function can be shaped to obtain particular characteristics while maintaining a constant envelope. One such characteristic is autocorrelation functions with increased peak-to-sidelobe distance, compared to that of the LFM counterpart. The infinite possible IF trajectories allow: construction of sets of orthogonal or uncorrelated signals for use in e.g. communication networks, communication with narrow-band interference [7], Multiple-Input and Multiple-Output (MIMO) communications [13] among other uses.

In this thesis only *continuous* NLFM chirps are considered. Looking at the Power Spectral Density (PSD) of the linear chirp in Figure 2.3, it is apparent that the PSD is rectangular. This comes from the fact that the PSD in a frequency range is proportional to the power of the chirp in that range. With equal bandwidth and constant envelope throughout the chirp, the PSD in a range is proportional to the chirp rate in that range. The LFM has a constant chirp range throughout the entire range, thus its PSD is "flat". The autocorrelation R_{ss} of a signal is the Inverse Discrete Fouriere Transform (IDFT) of its PSD.

$$\mathrm{R}_{ss}(\tau) = \mathcal{F}^{-1}\{S(f)\} \tag{2.9}$$

Shaping the PSD through the chirp rate, therefore shapes its autocorrelation through the Fourier relation. W. Doerry presents one method of doing just this [12]. Autocorrelation functions from known window functions can be obtained by shaping a LFM signal with a window function. Let $\gamma(t)$ be the chirp rate of a chirp signal for time $t \in \mathcal{T}$

$$\gamma(t) = \frac{\gamma(0)}{W(\omega(t) - \omega_0)}, \tag{2.10}$$

where $W(\cdot)$ is a window function, $\omega(t)$ is an LFM IF function, and $\omega_0 \coloneqq \omega(0)$ is the target center frequency.

A protocol for generating NLFM chirps with specific length, start and stop frequencies proposed in [12], is summarized here for clarity. From the target start and stop frequencies, and times, a prototype linear IF trajectory $\omega_{prototype}(t)$ is generated. From this function, a target bandwidth Ω_{target} is calculated using Equation 2.4. Now the NLFM IF path can be found be through Equation 2.10 with a scaled prototype IF path $a \times \omega_{prototype}(t)$.

$$\omega_{NLFM}(a,t) = \int \frac{\gamma(0)}{W((a \times \omega_{prototype}(t)) - \omega_0)}\,\mathrm{d}t \tag{2.11}$$

a must be set so that the target bandwidth Ω_{target} is met, i.e. the start and stop frequency is identical to that of the prototype IF path. The scaling factor a is found through an optimization technique as stated below.

$$a = \min_a \left|\Omega_{target} - \Omega_{NLFM}\left(\omega_{NLFM}(a,t)\right)\right| \tag{2.12}$$

A popular weighting function with a high peak-to-sidelobe distance is the Hamming window. A Hamming window is displayed in Figure 2.4, and a Hamming-weighted NLFM is displayed in Figure 2.5.

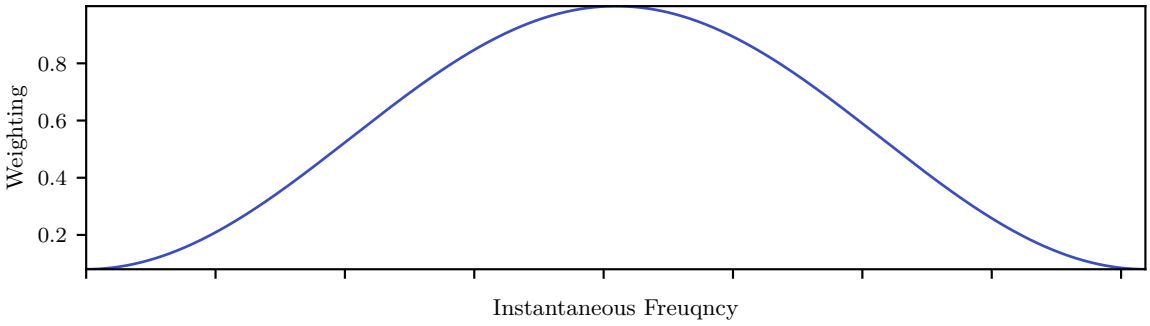

Figure 2.4: Hamming Window Weighting Function $W(\cdot)$

Figure 2.5 through 2.7 display a *continuous, non-linear* chirp in the time-domain, TF domain, and frequency domain respectively. The chirp has equivalent length and "chirp bandwith" Ω as the LFM signal in Figure 2.1.

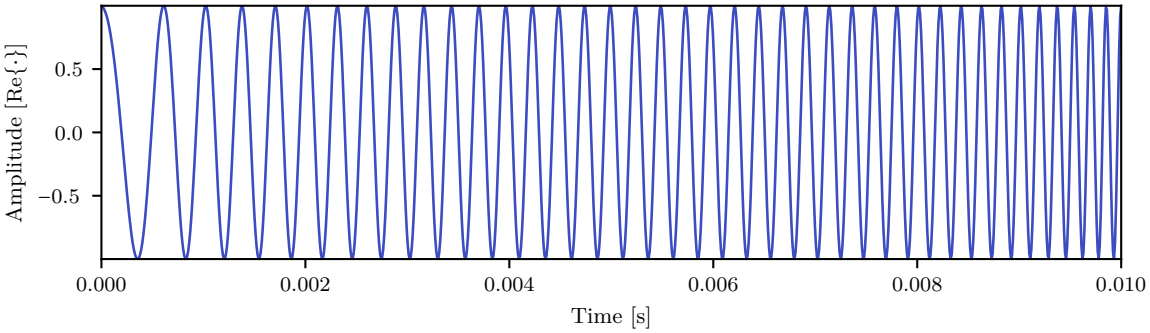

Figure 2.5: Constant Envelope Non-Linear Chirp in the time domain, $s(t)$

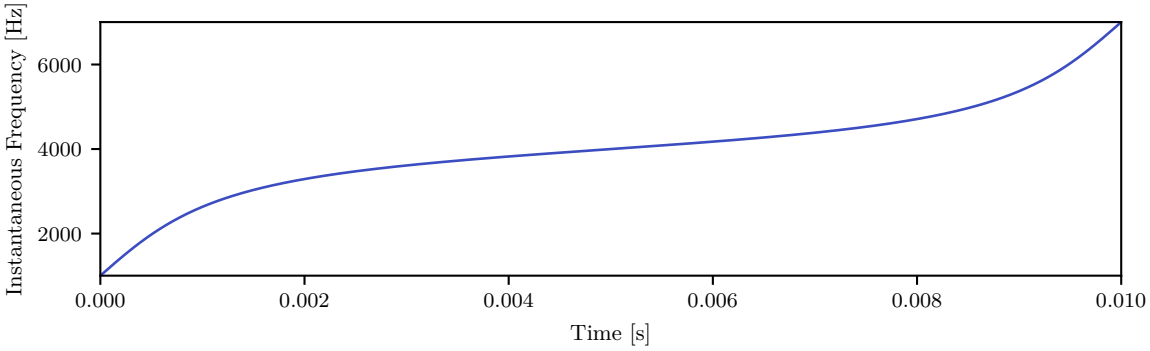

Figure 2.6: Angular Frequency $\omega(t)$ [Hz]

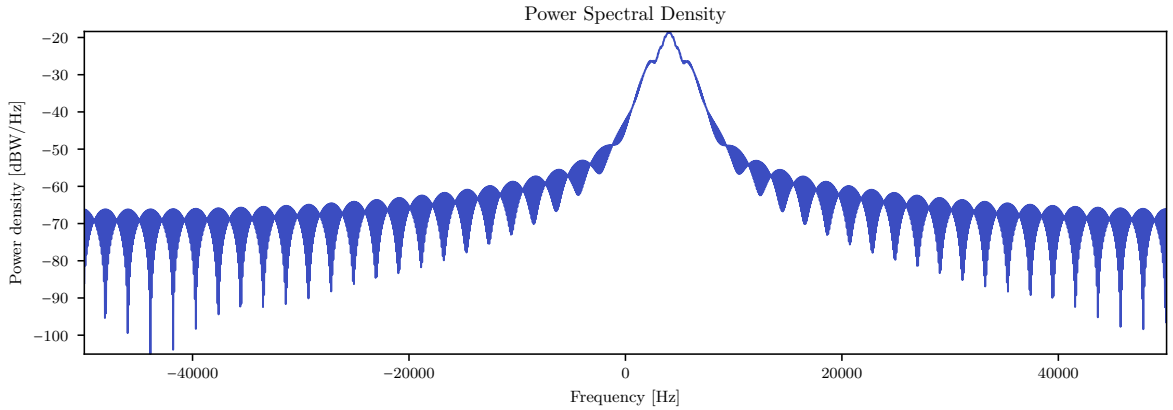

Figure 2.7: NLFM Periodogram

These chirps carry no information on their own. In order to be used for radio communications, they need some form of modulation.

2.1.1 Modulated Chirp Signals

There are multiple ways of modulating information on chirp waveforms. Similar to single tone communication schemes, one can apply on/off-keying or frequency shift keying (chirps with different starting frequencies representing different symbols). Complex modulations like Phase Shift Keying (PSK) and Quadrature Amplitude Modulation (QAM) can be modulated onto the chirp similarly to a single tone carrier [7]. Such signals are not explored in this thesis. By utilizing orthogonal chirps, M-ary communications is possible, where each symbol is represented by a dedicated chirp. The optimum filter for detection of a known signal is the *matched filter* [14]. This filter is in essence a correlator. In infinite SNR, the output of a matched filter applied the true symbol, is the autocorrelation of that symbol. An optimum matched filter receiver for an M-ary chirp communications scheme is displayed in Figure 2.8. For communications purposes, symbols should have a high autocorrelation peak-to-sidelobe ratio, and low cross-correlation [15], these characteristics are favorable to increase detection performance, and reduce incorrect symbol detection (symbol-error) in low SNR.

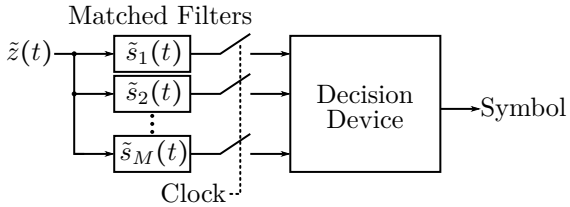

Figure 2.8: M-ary Chirp Receiver Architecture

LoRa is an M-ary chirp-per-symbol modulated communications physical layer standard [16], [17]. In LoRa, the symbols consists of linear chirps with a single chirp rate[†]. Each symbol has a dedicated starting frequency. Once the chirp reaches the maximum frequency, it wraps around to the minimum frequency. Below is an illustration of a symbol alphabet for a LoRa-like M-ary chirp-per-symbol modulation scheme. As can be seen from the IF symbol map, each symbol is a *linear, discontinuous* chirp.

[†]Except during IF wrap around.

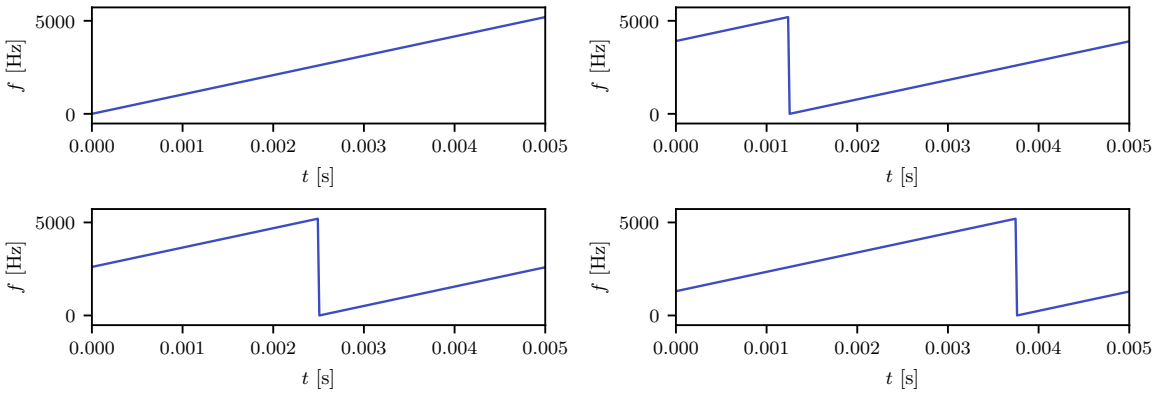

Figure 2.9: Linear Chirp Symbol Map ($M = 4$)

Digital communication receivers depend on synchronizing to the clock of the incoming signal to sample the symbols at the correct time (as can be seen from Figure 2.8). To ensure synchronization, communication packets are equipped with a synchronization sequence. This sequence is known by the receiver, typically a sequence with "favorable" autocorrelation properties. LoRa is a proprietary standard, so the knowledge of its physical layer relies on reverse engineering efforts. C. Bernier et al. have attempted to break down the synchronization sequences of LoRa [18]. Based on this paper, LoRa has an N-symbol preamble (where $N \in [2..2^{16}-1]$). It consists of complete chirps from f_{min} to f_{max}. This is followed by a two-symbol frame synchronization word (of identical symbols) and a 2.25 symbol *down-chirp* frequency synchronization sequence. Following the synchronization sequence are the headers and information symbols. Interested readers are referred to [18] for further details on the synchronization sequences of LoRa. Below is an illustration of a LoRa-like synchronization sequence.

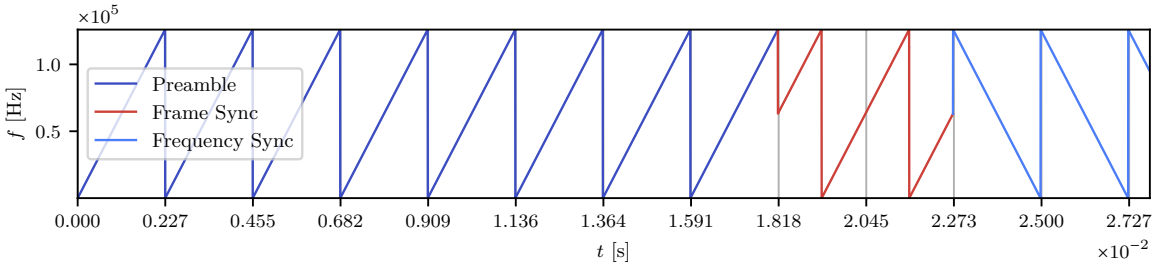

Figure 2.10: LoRa Synchronization Sequence. Grid Marking the Symbol Transitions.

The synchronization sequences are commonly static between packets, and as such they can be utilized in detection and estimation.

2.2 Signal-to-Noise Ratio

In a real world application the observed signal $\tilde{s}(t)$ would be distorted by noise. A typical observation model is

$$\tilde{z}(t) = \tilde{s}(t) + \tilde{w}(t), \tag{2.13}$$

where $\tilde{s}(t)$ is the target signal, and $\tilde{w}(t)$ is complex White Gaussian Noise (WGN). In order to quantify the quality of the observation an SNR is defined.

The SNR is a measure of the signal strength relative to a noise level. It is calculated as the ratio between the average signal power S, and the average noise power N.

$$SNR = \frac{S}{N} \tag{2.14}$$

The signal power S is defined as the average signal power throughout the signal duration T. The noise power N is defined as the average power of the noise process W over the observation duration. When the noise process is a Gaussian process $W \sim \mathcal{N}\left(\mu = 0, \sigma^2\right)$ (like in this thesis), then the noise power is

$$N \coloneqq \sigma^2. \tag{2.15}$$

For a complex noise process, the real and imaginary noise components are

$$\tilde{w} = w_{real} + iw_{complex}, \qquad w_{real} \sim \mathcal{N}\left(0, \frac{\sigma^2}{2}\right),\ w_{complex} \sim \mathcal{N}\left(0, \frac{\sigma^2}{2}\right). \tag{2.16}$$

The SNR is referred to in decibel form, as

$$SNR \coloneqq 10\log_{10}\left(\frac{S}{N}\right). \tag{2.17}$$

From Equation 2.14 it can be seen that the SNR gives no information on the noise density. A narrow-band signal in wideband noise can thus appear to be covered in noise, but can easily be extracted through a TF transform. In order to relate the signal to the noise density, a second relation is used; The normalized SNR. That is, the bit energy per noise power density per Hertz, defined as

$$\frac{E_b}{N_0} \coloneqq \frac{S \cdot B}{N \cdot f_s \cdot \log_2(M)}. \tag{2.18}$$

As the observation is distorted by noise, the *true* value of a parameters cannot be found. Trough various techniques called estimators, estimates of varying accuracy can be calculated.

2.3 Estimation

Estimation is the process of guessing the value of a parameter in the presence of some form of noise. The error of an estimate $\hat{\theta}$ of parameter θ is calculated as follows:

$$e = \theta - \hat{\theta} \tag{2.19}$$

The quality of an estimator can be measured by use of a loss function $L\{\cdot\}$, which in its simplest form is the Mean Absolute Error (MAE) [14, p. 115][‡]:

$$L_{MAE}\{\boldsymbol{e_i}\} = \frac{\|\boldsymbol{e_i}\|_1}{I} = \frac{\mathbb{1}^T|\boldsymbol{e}_i|}{I} \tag{2.20}$$

Here the mean absolute error is calculated for a set of I estimation occurrences.

Some estimators allow the use of *a priori* information. This is knowledge of the probable values of the parameter θ before computation. Say one is estimating the frequency of a complex exponential in the presence of noise, and the range for which the frequency θ is likely to occur is known. Using a Discrete Fouriere Transform (DFT)-based MLE method, one can apply a weighting $\boldsymbol{w}$ to the signal based on the prior information $\tilde{\boldsymbol{x_f}}' = \boldsymbol{w}\tilde{\boldsymbol{x_f}}^T$. One way of expressing the prior probabilities is by use of Gaussian Mixture Models (GMM) [19, ch. 3]. A GMM is a $\mathbb{R}^a$ model built of a set of $b \in \mathbb{N}$ Gaussians with weight ϕ.

$$p(\theta) = \sum_{i=1}^{b} \phi_i \mathcal{N}(\mu_i, \sigma_i) \tag{2.21}$$

[‡][14] presents the MAE simply as the 1-norm of the error vector.

2.4 Frequency Domain Estimation

The frequency content of an emission is a powerful parameter. Due to the physical laws of radiation, the frequency content reveals information about the physical size and technology of the transmitter. Second, knowledge of the frequency distribution of a signal can aid in the estimation of other parameters. Perhaps the most fundamental parameter in the frequency domain is the center frequency.

2.4.1 Center Frequency Estimation

The frequency of a complex exponential in WGN can be estimated through a ML method [20]. For a signal

$$\tilde{s}(t) = a(t)e^{i2\pi f_c t+\phi} \tag{2.22}$$

embedded in WGN $w(t)$, resulting in the observation

$$\tilde{z}(t) = \tilde{s}(t) + \tilde{w}(t), \tag{2.23}$$

the ML frequency estimator is

$$\hat{f}_{ML} = \arg\max_{f\in\Omega} |\tilde{Z}[f]|, \qquad \Omega = \left\{ k\frac{f_s}{K} \middle| k \in \mathbb{Z} \wedge -\frac{K}{2} \leq k < \frac{K}{2} \right\}, \tag{2.24}$$

where f_s is the sample frequency, K is the size of the DFT, and

$$\tilde{Z}[f] = \mathcal{F}\{\tilde{z}(t)\}. \tag{2.25}$$

The accuracy of the estimator in Equation 2.24 is proportional to the DFT size K, as the functions codomain Ω is bound to discrete values, which are fractions of the sampling frequency.

The DFT can be computed (computationally efficiently) through the Fast Fourier Transform (FFT) [21]. The complexity of this algorithm increases with $K \log_2 K$. With this algorithm, high accuracy estimators will require a substantial amount of computation, in addition to the peak search, where the computational complexity increases linearly with K. Duda shows that using windows on the sampled data with narrow main lobes can improve the accuracy, and noise immunity of the estimator [22].

A method of improving the accuracy to sub-bin resolution is that of the Quadratically-Interpolated FFT (QIFT) [23]. This method applies a quadratic interpolation around $\arg\max_{f\in\Omega} |\tilde{Z}(f)|$. By fitting

$$y = a_2x^2 + a_1x + a_0 \tag{2.26}$$

to

$$\left|\tilde{Z}[f]\right|\Big|_{f=\{f_{k_{ML}-1}, f_{k_{ML}}, f_{k_{ML}+1}\}}, \tag{2.27}$$

an estimate the center frequency in non-integer steps is obtained[§]. Equation 2.26 can be fitted through e.g. *least squares* as illustrated in Figure 2.11 [22], [25].

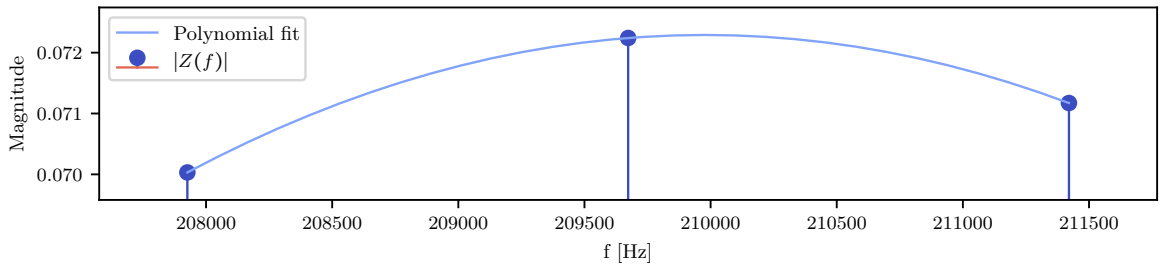

Figure 2.11: Quadratic Fit Around $\arg\max_{f\in\Omega} |\tilde{Z}(f)|$

[§]Additional methods of sub-bin frequency estimators can be found in [24]

The vertex of the interpolated parabola is the peak of the likelihood function. The estimator $\hat{f}$ then becomes

$$\hat{f} = \frac{-a_1}{2a_2}. \tag{2.28}$$

This allows greater accuracy without increasing the DFT size. The interpolated DFT MLE method described above is hereby denoted as the *DFT MLE method*.

2.4.2 Bandwidth Estimation

A second parameter that can be estimated in the frequency domain is the power bandwidth. For unknown pulses the bandwidth can be estimated through the PSD of the observation.

$$B(x) = f_{upper}^{x\,\mathrm{dB}} - f_{lower}^{x\,\mathrm{dB}} \tag{2.29}$$

The upper and lower band limits are the frequencies for which the PSD of the observation $P(f)$ has fallen $x\,[\mathrm{dB}]$ from its peak.

$$\lim_{f \to f_{lower}^{+}} \left| 10\log_{10} P(f) - \lambda(x) \right| = 0, \tag{2.30}$$

$$\lim_{f \to f_{upper}^{-}} \left| 10\log_{10} P(f) - \lambda(x) \right| = 0, \tag{2.31}$$

where

$$\lambda(x) = \left[10\log_{10} \max P(f) \right] - x\,[\mathrm{dB}]. \tag{2.32}$$

Equation 2.30 and 2.31 is solved for f_{lower} and f_{upper} respectively. This assumes that the $x\,[\mathrm{dB}]$ threshold is crossed only once at each side of the center frequency. By studying Equation 2.30 and 2.31 it can be seen that this estimator only works when the PSD peak is $> x\,[\mathrm{dB}]$ above the "noise floor".

Through these methods, the peak of the magnitude spectrum and power bandwidth can be estimated, however, a chirp has a frequency that changes with time. The time-dependent frequency, or *Instantaneous Frequency* can also be estimated.

2.5 Instantaneous Frequency Estimation

The IF is a key parameter of the chirp, from which many other parameters can be calculated. There has been a lot of research on instantaneous frequency estimation. Some historical and modern methods are therefore studied.

2.5.1 Direct Estimation

The *direct* methods are those estimators that do not rely on any transformation of the observation prior to estimation. The instantaneous frequency of a time series as defined in Equation 2.2 can be calculated as follows:
Let $s(t)$ be a signal consisting of a complex exponential $s(t) = a(t)e^{i\Phi(t)}$. The instantaneous frequency $\omega(t)$ is defined as

$$\omega(t) := \frac{1}{2\pi} \frac{\mathrm{d}\Phi(t)}{\mathrm{d}t}\,[\mathrm{Hz}]. \tag{2.33}$$

A phase estimate of an observation will be in the range $[-\pi, \pi\rangle$. Once the phase supersedes the range, it wraps around. This wraparound causes phase ambiguities which breaks the IF estimate (see Figure 2.12).

A. E. Barnes proposes the computationally efficient *two-point FIR* IF estimator, which is unaffected by these phase ambiguities [26]. Let

$$\tilde{s}(t) = x(t) + iy(t) \tag{2.34}$$

denote the real and imaginary part of the signal $\tilde{s}(t)$. The *Barnes method* is

$$\hat{\omega}(t) = \frac{1}{T_s} \tan^{-1}\left(\frac{x(t)y(t+T_s) - x(t+T_s)y(t)}{x(t)x(t+T_s) + y(t+T_s)y(t)}\right) [\text{rad}]. \tag{2.35}$$

Barnes might not have been aware of the possibility of *unwrapping* the phase prior to estimating the IF. Phase unwrapping is the process of ensuring that the phase is continuous $\Delta\Phi < \pi$. This is accomplished by successively adding or subtracting 2π recursively from non-compliant samples until they have $\Delta\Phi < \pi$. Figure 2.12 displays the phase ambiguities of a wrapped phase, and the corresponding unwrapped phase trajectory.

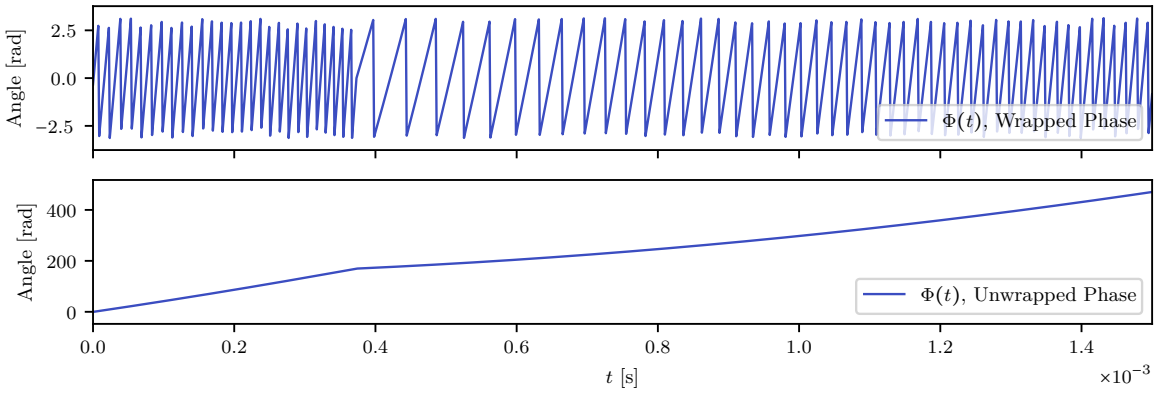

Figure 2.12: Wrapped and unwrapped phase functions $\Phi(t)$ for a LoRa-Like Symbol

Knowing this, the IF can be estimated as

$$\hat{\omega}(t) = \frac{\mathrm{d}\,\mathrm{unwrap}\left(\arg(\tilde{s}(t))\right)}{\mathrm{d}t} [rad], \tag{2.36}$$

In the case of a sampled time series, the signal $s[n] = s(t)\big|_{t=nT_s}$ will have phase ambiguities for frequency components which have a frequency $|f| > \frac{f_s}{2}$. For such components, the phase between adjacent samples will be $s[(n+1)T_s)] - s[nT_s] > \pi$, and will cause aliasing, even when phase unwrapping is applied.

The two "direct" methods above offer little noise rejection. An approach with greater noise rejection is through a TF transform. A TF distribution spreads the noise out in time and frequency as a pseudo noise suppression. The IF can be estimated through TF transforms such as a WVD [27] and *Hilbert Spectrum* [28][¶]. All TF transforms have limitations with regards to the TF function codomain or generality of excitation signals. Hilbert et al. presents a thorough comparison of some of these issues in his paper introducing the HHT [28].

2.5.2 The Wigner-Ville Distribution

The WVD is a TF distribution which is able to obtain greater time resolution than the well known spectrogram. It is a special case of *Cohens* general class of time frequency distributions [31]. The WVD

[¶]Some of the methods not covered in this thesis is the spectrogram [29], scalarogram [30]

is the Fourier integral of the central covariance function [31], [32]

$$W(\omega, t) \coloneqq \int_{-\infty}^{\infty} C_c(\tau, t) e^{-i\omega\tau} \, \mathrm{d}\tau, \tag{2.37}$$

where $C_c(\tau, t)$ is the central covariance function of a time series $\tilde{s}(t)$ defined as

$$C_c(\tau, t) \coloneqq \tilde{s}(t - \frac{1}{2}\tau)\tilde{s}^*(t + \frac{1}{2}\tau). \tag{2.38}$$

The resulting is a time-frequency distribution of the signal, as displayed in Figure 2.13.

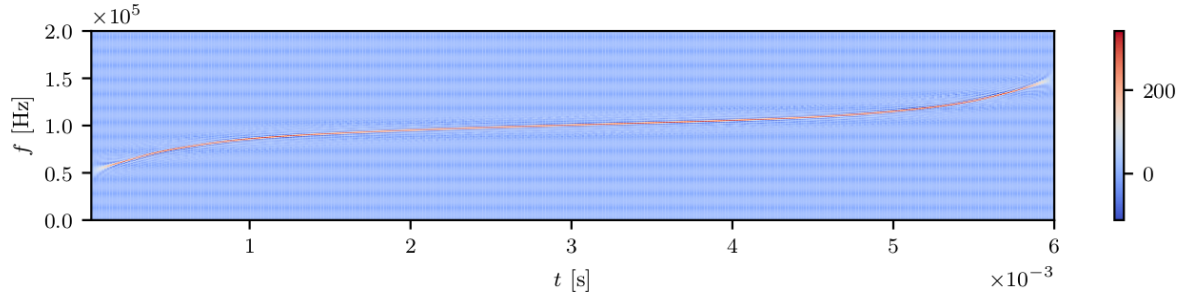

Figure 2.13: $W_{\tilde{s}}(\omega, t)$, $\frac{S}{N} = 10\,\mathrm{dB}$

The WVD suffers from so-called *cross terms*. These are the result of cross WVD of two signals. Let W_{11} and W_{22} be the WVD of signals $s_1(t)$ and $s_2(t)$ respectively. The WVD of signal

$$s(t) = s_1(t) + s_2(t), \tag{2.39}$$

found by substituting Equation 2.39 into 2.37 is [31, ch. 8]

$$W(t, \omega) = W_{11}(t, \omega) + W_{22}(t, \omega) + W_{12}(t, \omega) + W_{21}(t, \omega) \tag{2.40}$$

$$= W_{11}(t, \omega) + W_{22}(t, \omega) + 2\,\mathrm{Re}\left\{W_{12}(t, \omega)\right\}. \tag{2.41}$$

The last term in Equation 2.41 is the *cross term*. The cross-terms lie between the two signal components, and as shown above; Its magnitude can be twice that of the individual components [27]. The cross-terms become apparent when applying a chirp symbol like described in subsection 2.1.1. This can be seen in Figure 2.14 in the time range $[0.2, 0.6]\,[s]$[‖]. Note how the cross term shifts from red to blue in an oscillatory behavior.

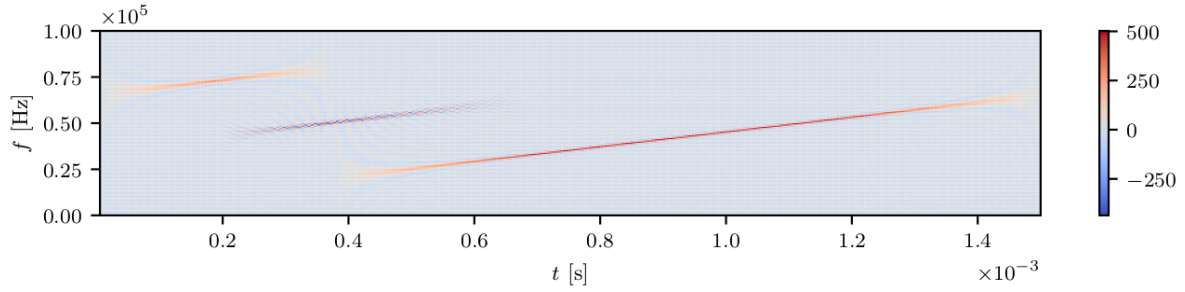

Figure 2.14: $W_{\tilde{s}}(\omega, t)$, LoRa-Like Symbol with Cross Terms

[‖]Readers might notice the shorter pulses. The shorter signal is used for visual purposes.

In Equation 2.37 there is an infinite integral, which for the Discrete Wigner Distribution (DWD) becomes an infinite sum. To overcome this, the signal is windowed in what is called the Pseudo Wigner Distribution (PWD). Its discrete implementation is [33]

$$W[l,\omega] = 2\sum_{n=-N-1}^{N-1} f_l[n]e^{-i2\omega n}, \tag{2.42}$$

where

$$f_l[n] = \tilde{z}[l+n]\tilde{z}^*[l-n]w[n]w[-n], \tag{2.43}$$

ω is the angular frequency periodic around $\frac{f_s}{2}$, and $w[n]$ is a window of length $2N-1$, with the constraint $w(0) = 1$. This window can be utilized to reduce cross terms. This window does not affect the time resolution, but does reduce the frequency resolution [33]. Such windowing is often implied when using the term PWD. The term WVD is used in this thesis to state explicitly that there is no frequency smoothing window applied. That is, a window of $\mathbb{1}$ is used. This reduces Equation 2.42 and 2.43 to[**]

$$W[l,\omega] = 2\sum_{n=-N-1}^{N-1} \tilde{z}[l+n]\tilde{z}^*[l-n]e^{-i2\omega n}. \tag{2.44}$$

A computationally efficient implementation can be found in [35]. Interested readers are referred to [31] for further details on the WVD.

The WVD is widely describes in the literature for IF estimation. Using MLE on the WVD is an *efficient* IF estimator for *continuous linear* chirps in a constrained SNR range [27], [36]. The method finds the IF $\omega(t)$ that maximizes the likelihood function $\mathcal{L}(\omega|\tilde{z}(t)) = W_{\tilde{z}}(t,\omega)$.

$$\hat{\omega} = \arg\max_{\omega} \mathcal{L}(\omega|\tilde{z}(t)), \tag{2.45}$$

2.5.3 Hilbert Spectrum

Huang et al. proposes a method of generating a spectrum with as great of a time resolution as the WVD, but without the destructive cross terms [28]. This method hereby called the HHT consists of decomposing the observation into its Intrinsic Mode Functions (IMFs)[††]. The EMD as presented in [28] only decomposes real signals, however complex signals can be decomposed using the "bivariate" EMD of Rilling et al. [38]. Only real EMDs are considered in this thesis. Interested readers are referred to [28], [37], [39] for details on the algorithm.

The signal is decomposed successively by extracting its *mono-component oscillatory modes* [40] (IMFs). Once a component is extracted, it is subtracted from the observation, and the process repeats until a stopping criterion is met. The signal can thus be expressed as a sum of N real IMFs and a residue [28].

$$s(t) = \sum_{i=1}^{N} c_i(t) + r_n(t) \tag{2.46}$$

Figure 2.15 displays the IMFs for the real part of an NLFM chirp signal, extracted using the *sifting* algorithm with stopping criterions $\phi_1 = 0.05$, $\phi_2 = 0.5$ and $\alpha = 0.05$ from [39][‡‡].

[**]The equation on this form is presented as the "Discrete Wigner Distribution" in [34].

[††]This process called Empirical Mode Decomposition (EMD) is computed through the *Sifting algorithm* [37].

[‡‡]The EMD is computed by the *pyhht* python implementation [41].

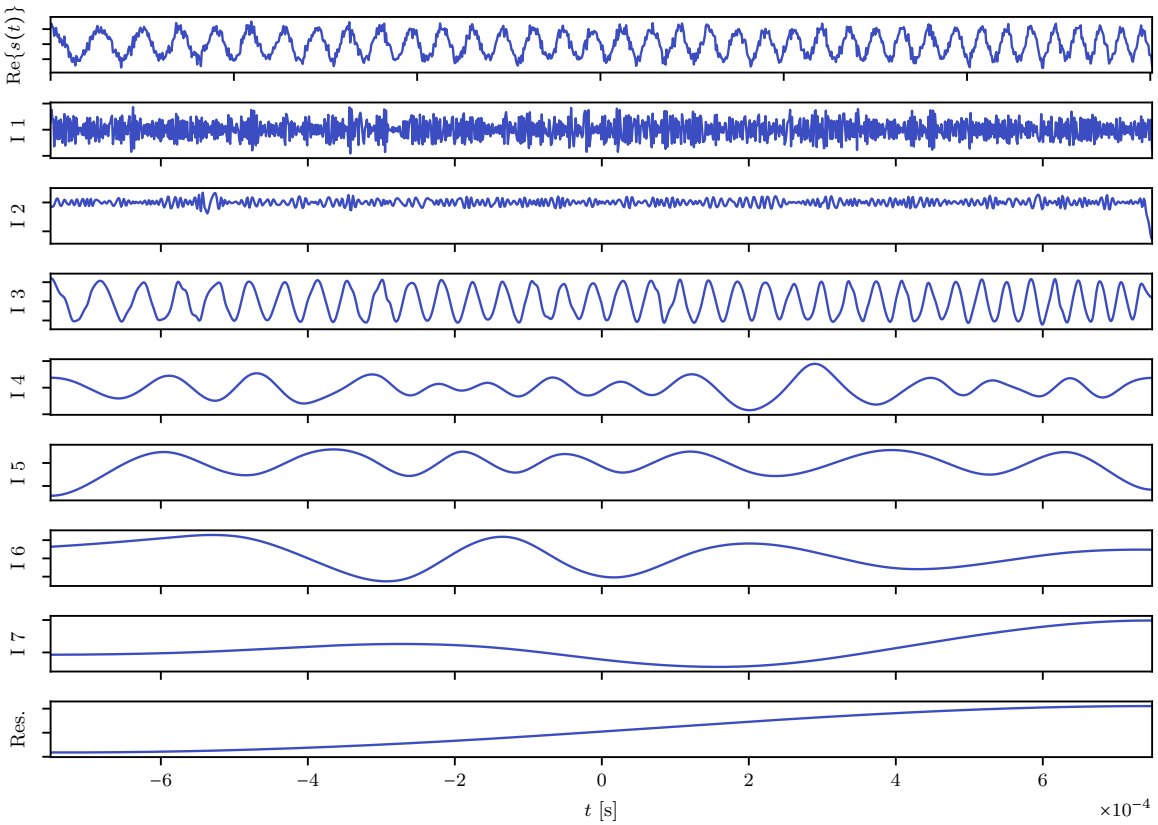

Figure 2.15: NLFM Chirp Decomposed to its IMFs with Residue Using the *Sifting* Algorithm.

From the series of Equation 2.46, one can compute the *Hilbert amplitude spectrum* $H(\omega, t)$ hereby denoted as the *Hilbert spectrum*. First the *analytical* signal is computed for each component (and residue) through the *Hilbert Transform*.[§§] The Hilbert transform is defined as

$$\check{s}(t) \coloneqq \frac{1}{\pi t} \circledast s(t). \tag{2.47}$$

The IF $\omega_n(t)$ of each analytical component

$$\check{s}(t) = \sum_{i=1}^{N} \check{c}_i(t) + \check{r}_n(t), \tag{2.48}$$

is estimated using Equation 2.36. The magnitude of each component is obtained directly from the analytical components as

$$a_i(t) = \left|\check{c}_i(t)\right|. \tag{2.49}$$

The polar representation of the signal

$$\tilde{s}(t) = \mathrm{Re}\left\{\sum_{i=1}^{N} a_i e^{i\int \omega_i(t)\,\mathrm{d}t} + a_r e^{i\int \omega_r(t)\,\mathrm{d}t}\right\} \tag{2.50}$$

[§§]The Hilbert transform is a way of transforming a real signal into a complex or *analytical* signal. While the real signal only has a single component $\boldsymbol{\Theta}$, the analytical signal has a real and imaginary component: $\tilde{s}(t) = \mathrm{Re}\{\tilde{s}(t)\} + i\,\mathrm{Im}\{\tilde{s}(t)\}$.

is used to generate the *Hilbert spectrum* . $H(\omega, t)$ is obtained by plotting the components (modes and residue) along time t, frequency $f\big|_{f=\frac{\omega}{2\pi}}$ and magnitude a. The transform has been adapted for various tasks in SEI [42]–[44]. A resulting spectrum for the troublesome LFM symbol is displayed below[¶¶].

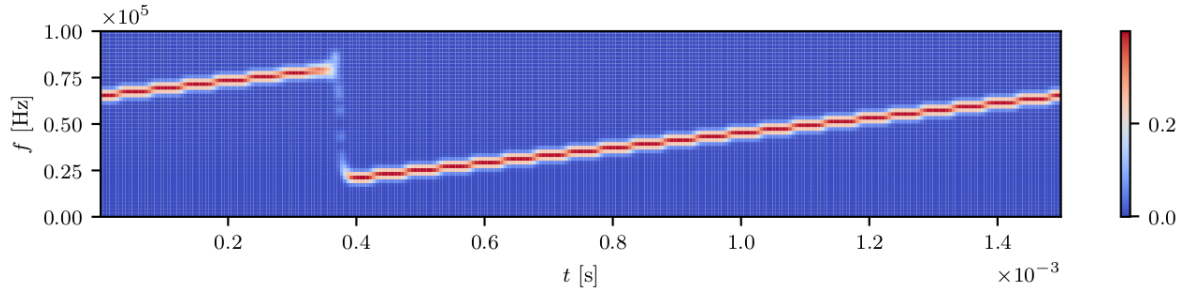

Figure 2.16: $H_{\tilde{s}}(f, t)$, LoRa-Like Symbol

One method of estimating the instantaneous frequency based on the Hilbert spectrum is that of the MLE. Let

$$\mathcal{L}(\omega|\tilde{z}(t)) \coloneqq H_{\tilde{s}}(\omega, t) \tag{2.51}$$

be the likelihood function for instantaneous frequency $\omega(t)$ given observation $\tilde{z}(t)$. The MLE for the IF is

$$\hat{\omega} = \arg\max_{\omega} \mathcal{L}(\omega|\tilde{z}(t)). \tag{2.52}$$

The method above essentially estimates the IF twice, first for each component, and then based on the likelihood function of Equation 2.51 (which is the distribution of the IF estimates for the components). And as such it is a pseudo multi-component variant of Equation 2.36.

2.5.4 Polynomial Phase Trajectory Modeling

A method suitable for *continuous* chirps is that of *polynomial phase trajectory modeling*. This method utilizes *a priori* information on how rapidly the signal is changing through the use of a phase polynomial. It is unbiased for continuous NLFM chirps down to low SNR [36]. Polynomial IF estimators can be applied to the WVD [45] or directly to the signal in time domain. The latter is studied further. This method is deemed too compute-intensive for practical use in [36]. Since then, the computing cost with regards to power and time, have decreed manifold. Therefore a revisit seems suitable. Let a signal $\tilde{s}(t)$ be defined as

$$\tilde{s}(t) = a(t)e^{i\Phi(t)}, \tag{2.53}$$

where $\Phi(t)$ is a polynomial of order P,

$$\Phi(t) = a_0 + a_1 t + a_2 t^2 + ... + a_P t^P, \qquad P \in \mathbb{N}, \tag{2.54}$$

and observation

$$\tilde{z}(t) = \tilde{s}(t) + \tilde{w}(t) \tag{2.55}$$

is the observed signal in noise. The polynomial coefficients can be estimated using linear least square techniques. This method will meet the Cramer-Rao Lower Bound (CRLB) in high SNR [36]. A second

[¶¶]The low frequency resolution is a consequence of the image discretization.

method is the ML polynomial coefficient estimation. This last method is shown to be superior with regards to performance in low SNR. The MLE polynomial coefficients are estimated as follows: Boashash shows that the likelihood function for the parameter vector $\boldsymbol{\alpha} = [A, a_0, a_1, .., a_P]^T$ given the observation $\tilde{z}(t)$ can be reduced to [36]

$$\mathcal{L}(\boldsymbol{\alpha}|\tilde{z}(t)) = 2A\,\mathrm{Re}\Big\{e^{-ia_0} D(a_1, a_2, .., a_P)\Big\} - A^2 \tag{2.56}$$

where $x(t)$ is the real, and $y(t)$ the imaginary component of $\tilde{s}(t)$, and

$$D(a_1, a_2, .., a_P) = \langle z(t) e^{-i(a_1 t + a_2 t^2, .., a_P t^P)} \rangle_T. \tag{2.57}$$

The magnitude scalar A and the coefficient vector $\boldsymbol{a}$ is found by maximization of the likelihood function $\mathcal{L}(\cdot)$.

$$\hat{\boldsymbol{\alpha}} = \arg\max_{\boldsymbol{\alpha}} \mathcal{L}(\boldsymbol{\alpha}|\tilde{z}(t)) \tag{2.58}$$

The IF estimator is

$$\hat{f}(t) = \frac{1}{2\pi} \sum_{p=1}^{P} p\hat{a}_p t^{p-1}. \tag{2.59}$$

A. W. Doerry shows that polynomial reconstruction of NLFM chirps require a phase polynomial of sizes in the range $P = [4..12]$ [12]. These estimators can estimate the curve of a single chirp. In radio packets or pulse trains, multiple pulses are transmitted in conjunction. In order to separate the symbols or pulses, knowledge on the pulse, or symbol period is necessary. In communications, these pulses generally have identical symbol period for all symbols. As such they contain *cyclic* properties.

2.6 Cyclostationary Processes

A Cyclostationary (CS) process is a process for which its Higher Order Moments (HOMs) are periodic (cyclic). A process x is second-order CS in the wide sense if its mean $\mathbb{E}\{x(t)\}$ and autocorrelation $\mathrm{R}_{xx}(t, \tau)$ are periodic around some period T [46], [47, p. 5]

$$\mathbb{E}\{x(t)\} = \mathbb{E}\{x(t+T)\} \tag{2.60}$$

$$\mathrm{R}_{xx}(t, \tau) = \mathrm{R}_{xx}(t+T, \tau) \tag{2.61}$$

Communication signals have strong CS properties with a fixed symbol period T. Figure 2.17 displays the autocorrelation of a pulse train of NLFM pulses. An apparent cyclic nature in the peaks of the autocorrelation can be seen.

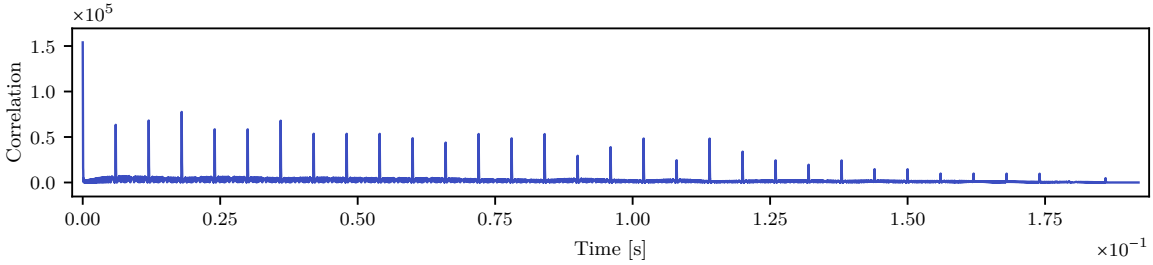

Figure 2.17: Autocorrelation $\left|\mathrm{R}_{\tilde{s}\tilde{s}}(t)\right|$ of a 32-Bit NLFM Chirp-Per-Bit Signal

CS analysis is gaining traction in modulation detection and MR due to its robustness to noise and interference [1], [11]. The cyclic properties of a CS processes can be analyzed in time and frequency

domain through the Spectral Correlation Density (SCD) and the Cyclic Autocorrelation Funcion (CAF) respectively. The latter is not considered in this thesis. The SCD is defined as

$$S_{\tilde{x}\tilde{x}^*}(\alpha, f) \coloneqq \lim_{\Delta f \to 0} \lim_{T \to \infty} \left\langle \mathbb{E}\{\Delta \tilde{X}_{1/\Delta f}(t, f) \tilde{X}^*_{1/\Delta f}(t, f - \alpha)\} \right\rangle_T, \tag{2.62}$$

were $X_Z(t, f)$ is the Short-Time Fourier Transform (STFT), defined as

$$X_Z(t, f) \coloneqq \int_{t-Z/2}^{t+Z/2} x(s) e^{-i2\pi f s} \, \mathrm{d}s. \tag{2.63}$$

$S_{\tilde{z}\tilde{z}^*}(\alpha, f)$ represents the correlation of spectral components at frequencies f and with the cycle-frequency α. For $\alpha = 0$, then $S_{\tilde{z}\tilde{z}^*}(0, f)$ reduces to the PSD of $\tilde{z}(t)$. A Wide Sense Stationary (WSS) process like WGN is not CS, and will not have an α distribution. An illustration of a SCD is displayed in Figure 2.18. It shows the distribution of a pulsed communication signal. Communications signals with a constant symbol period have strong CS features which can be seen along the α axis.

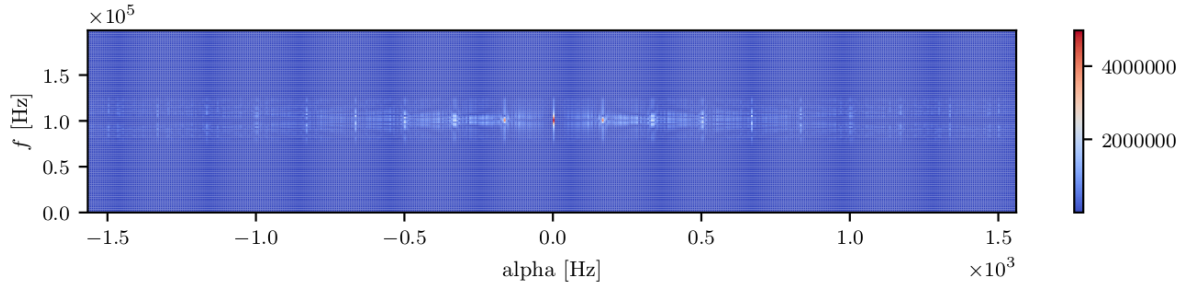

Figure 2.18: Spectral Correlation Density Estimate $\left|\hat{S}_{\tilde{s}\tilde{s}^*}(\alpha, f)\right|$ of a 32-bit binary NLFM packet (Positive Frequencies Only)

The *conjugate* SCD is simply the SCD with the second STFT term non-conjugated $S_{\tilde{x}\tilde{x}}(\alpha, f)$. Figure 2.19 displays the *conjugate* SCD of a signal as above.

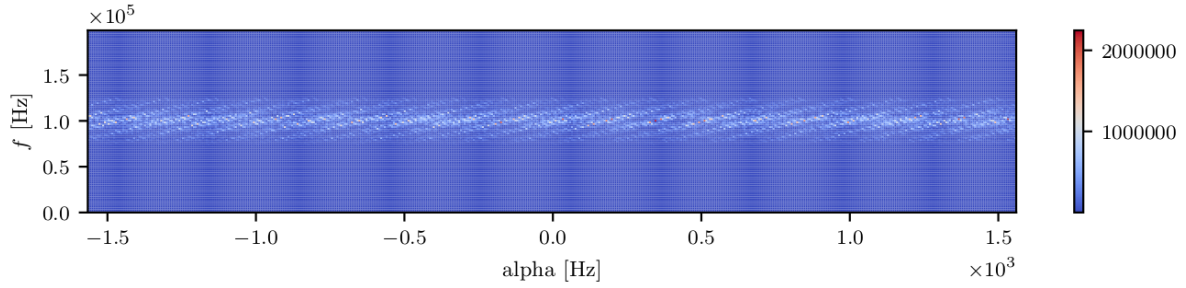

Figure 2.19: *Conjugate* Spectral Correlation Density Estimate $\left|\hat{S}_{\tilde{s}\tilde{s}}(\alpha, f)\right|$ of a 32-bit binary NLFM packet (Positive Frequencies Only)

For discrete time signals the SCD of Equation 2.62 can be estimated (computationally efficient) through the FFT Accumulation Method (FAM) [48]. It is defined as[***]

$$S^{\alpha_i + q\Delta\alpha}_{\tilde{x}\tilde{x}^*}[n, f_j]_{\Delta t} \coloneqq \sum_r \tilde{X}_T[rL, f_k] \tilde{X}^*_T[rL, f_l] g_c(n - r) e^{-i2\pi rq/P}, \qquad L, N, P \in \mathbb{N} \tag{2.64}$$

[***]A two-dimensional "FFTshift" is necessary for $S_{\tilde{x}\tilde{x}^*}(nL, f_j)$ to go from $\left[-\frac{f_s}{2}, -\frac{f_s}{2} + \Delta f, \ldots, \frac{f_s}{2} - \Delta f\right]$, $\left[-\frac{L}{2}\Delta\alpha, -\left(\frac{L}{2} - 1\right)\Delta\alpha, \ldots, \left(\frac{L}{2} - 1\right)\Delta\alpha\right]$.

where:
$\Delta t = N/f_s$ is the period of the observation.
N is the length of the input. It defines the cycle-frequency resolution

$$\Delta\alpha = \frac{f_s}{PL}. \tag{2.65}$$

N must be of length $L \times N'$, and is subject to $L << N$.
$P = N/L$.
L is an integer specifying the cycle-frequency range.
$g_c(\cdot)$ is a data selection window. E.g. a rectangular window $\mathbb{1}$ of length L.
$\alpha_i = f_k - f_l$.

$$X_T[n, f] = \sum_{r=-N'/2}^{N'/2-1} a[r]x[n-r]e^{-i2\pi f[n-r]T_s}, \qquad N' \in \mathbb{N} \tag{2.66}$$

where N' is an integer specifying the channelization (frequency) resolution

$$\Delta f = \frac{f_s}{N'}, \tag{2.67}$$

and $a(\cdot)$ is a tapering window for the channelization. The window is of length N'.

Based on this frequency-cycle-frequency transform, signal parameters can be estimated.

2.7 Fundamental Frequency Estimation

Let

$$s(t) = \sum_{r=1}^{R} a_p e^{i2\pi r f_0 + \Phi_r} \tag{2.68}$$

be a harmonic signal consisting of a fundamental $s(t)\big|_{r=1}$ with frequency f_0, and $R-1$ harmonic tones. For a sampled harmonic signal $s[n] = s(t)\big|_{t=nT_s}$, the fundamental frequency f_0 can be estimator through a ML method. Wise et al. proposes a method of finding the fundamental frequency that maximizes the signal energy of a periodic signal [49]:

$$\hat{p} = \arg\max_p \frac{2P}{K_0} \sum_{l=1}^{N-1} \left|\mathrm{R}_{\tilde{z}\tilde{z}}[lp]\right|, \qquad p \in \mathbb{R}, \tag{2.69}$$

where K_0 is the length of the discrete signal, $N = \frac{K_0}{P}$, and P is the period of the sequence. The autocorrelation is defined as

$$\mathrm{R}_{\tilde{z}\tilde{z}}[k] := \sum_{j=0}^{K_0-1-k} r_j k_{j+k}. \tag{2.70}$$

The estimate of the fundamental frequency is $\hat{f}_0 = \frac{1}{\hat{p}T_s}$. This method can estimate the period p to an accuracy beyond the sampling period. This is accomplished by allowing p to be any real number ($p \in \mathbb{R}$) with the constraint that pl is rounded to the nearest integer $\lfloor lp + \frac{1}{2} \rfloor$. Wise et al. applies a weighting in Equation 2.69 that weighs the longer periods equally as the short [49]. Without this weighting, the estimator becomes

$$\hat{p} = \arg\max_p \sum_{l=1}^{N-1} \left|\mathrm{R}_{\tilde{z}\tilde{z}}\left[lp\right]\right|, \qquad p \in \mathbb{R} \tag{2.71}$$

$$\text{subject to} \quad lp \in \mathbb{Q} \tag{2.72}$$

Figure 2.20 shows the sum of Equation 2.71 for the autocorrelation displayed in Figure 2.17 with different periods p. The symbol rate estimate would be the arg max of the sum.

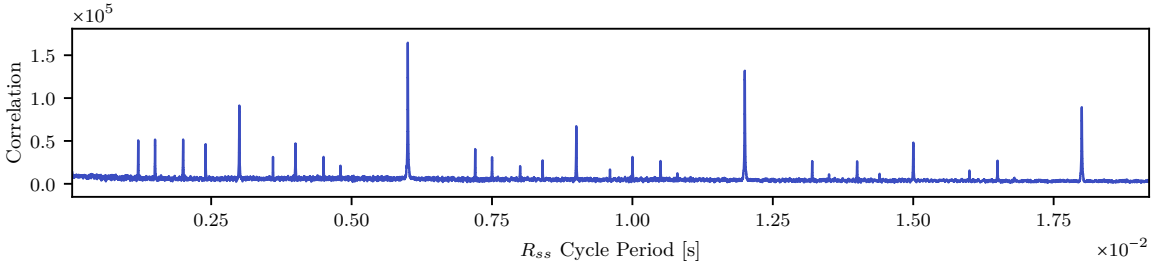

Figure 2.20: Cyclic period of a 32-Bit NLFM Chirp-Per-Bit Signal

2.8 On the Discrete Fourier Transform and its Frequency Response

The DFT is a time-to-frequency transform. It can be used to calculate the frequency content of a vector or time series. The DFT is defined as[†††] [50, p. 468]

$$\tilde{Z}[k] := \sum_{n=0}^{N-1} \tilde{z}[n] e^{-\frac{i2\pi}{N} kn}, \qquad k = [0..N-1], \tag{2.73}$$

where $\tilde{z}[n]$ is a time series, and $\tilde{Z}[k]$ is the resulting discrete coefficients in the frequency domain.

The DFT is equivalent to a filter bank of N filters, where

$$h[n] = \begin{cases} 1, & 0 \le n < N \\ 0 & \text{else} \end{cases} \tag{2.74}$$

is the Finite Impulse Response (FIR) low-pass coefficients for the filter of each bin. Each bin thus has a non-zero bandwidth set by $h[n]$. The response of the filter can be represented in the $\mathcal{Z}$-domain as the sum of the geometric series $H(Z) = 1 + z^{-1} + \cdots + z^{-(N-1)}$, which is

$$H(z) = \frac{1 - z^{-N}}{1 - z^{-1}}, \tag{2.75}$$

where $H(z) = \mathcal{Z}\left\{h[n]\right\}$. Its frequency response is [50]

$$H(\omega) = H(z)\big|_{z=e^{i\omega}} = e^{-i\omega\frac{N-1}{2}} \frac{\sin\left(N\omega/2\right)}{\sin\left(\omega/2\right)}, \tag{2.76}$$

where $\hat{\omega}_k = 2\pi\frac{k}{N}$ is the angular frequency per bin. The frequency response of a 10-point DFT bin is displayed below.

[†††]The DFT can be calculated efficiently by use of the FFT algorithm [21]

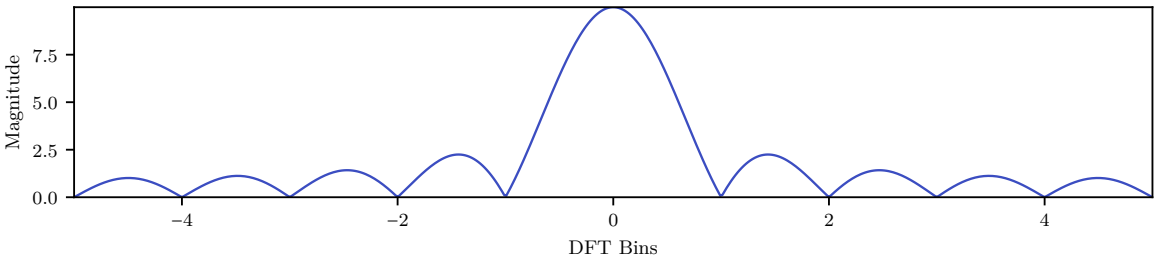

Figure 2.21: Frequency Response of DFT Bins $H(k)$ for a 10-point DFT

Chapter 3

Method

The performance of the estimators in this thesis is measured through statistical analysis. To ensure the quality of the analysis, a large number of Monte-Carlo runs are performed. A substancially lower amount of Monte Carlo iterations are used for vector estimators, as the implemented vector estimators consist of a series of scalar estimates.

3.1 Signal Generation

3.1.1 Discontinuous Linear Chirp

Linear chirps are constructed by creating a linear IF function $\omega(t)$ ranging from f_{min} to f_{max}. The function is windowed in time-domain by a rectangular window. From this, the phase path can be calculated by use of the relation in Equation 2.2. The signal $\tilde{s}(t)$ is constructed using Equation 2.1. By solving Equation 2.2 for Φ and substituting it and Equation 2.3 into Equation 2.1, the signal is expressed as

$$\tilde{s}(t) = a(t)e^{i\int 2\pi f(t)\,\mathrm{d}t}, \qquad t \in [-\frac{T}{2}, \frac{T}{2}\rangle \tag{3.1}$$

Modulated linear chirp signals are assembled by delaying and wrapping the signal $\tilde{s}(t)$ of Equation 3.1 in order to obtain an M-symbol alphabet.

$$\tilde{s}_m(t) = \tilde{s}(t')\Big|_{t'\in\left[\frac{Tm}{M}, T+\frac{Tm}{M} \mod \frac{T}{M}\right\rangle\Big| T'=T}, \qquad m = [0..M-1] \tag{3.2}$$

Where T' is the length of the interval for t. The resulting is an M-ary symbol alphabet, which with four symbols has an IF path similar to that displayed in Figure 2.9. The discontinuous linear chirp packets are assembled from a four-symbol alphabet in this thesis. The quality of the symbol alphabet is measured through a cross symbol dot-product. The dot-product of two sequences is equivalent to the cross-correlation at complete overlap. Figure 4.1 represents the expected correlation during the sampling for a perfectly synchronized matched filter receiver (like that of Figure 2.8). The "cross dot-product" is illustrated with a symbol product matrix

$$\boldsymbol{D}_{mn} = \boldsymbol{s}_m \cdot \boldsymbol{s}_n, \qquad m, n = [1..M], \tag{3.3}$$

where M is the number of symbols in the alphabet.
In packet construction, the symbols are appended as modulated time series. As a result, the phase at each IF is equal, independent of the symbol and subsequent starting frequency. For the linear chirp case, a LoRa-like synchronization sequence is added to the beginning of every packet. Let $s_m(t)$ be

symbol $m \in [0..M-1]$ with $M = 4$, and M_4 is the "down chirp" used for synchronization only. Then the synchronization sequence symbol stream is

$$\boldsymbol{q} = \left[s_0, s_0, s_0, s_0, s_0, s_0, s_0, s_0, s_1, s_1, s_4, s_4, s_4\big|_{t\in[0,0.25T\rangle} \right], \tag{3.4}$$

where the last symbol is only a quarter symbol period long. For packets including a synchronization sequence, the total length is $31.25 \times T_s$ s. These packets are thus slightly shorter than the 32 symbol long NLFM, and LFM packets without the sequence.

3.1.2 Continuous Non-Linear Chirp

NLFM chirp signals are generated using the method of Doerry [12] with Equation 2.12 and 2.11. The scaling parameter of Equation 2.12 is found through a Broyden-Fletcher-Goldfarb-Shanno (BFGS) optimization approach*. The symbol alphabet consists of an up chirp and the inverse down chirp. Both symbols have an initial phase of $\Phi(-\frac{T}{2}) = 0$. In contrast to the time-rotation method above, only two symbols are assembled from the IF path (a binary scheme). The communication packets consist of a random 32-bit sequence, where a "one" is represented by an up chirp, and a "zero" is represented by a down chirp.

3.2 Instantaneous Frequency Estimation

The IF path of the symbols are estimated using several techniques in order to compare, and measure their performance. The frequency is estimated as $f_{IF} = \omega/2\pi$. The estimators are excited with an NLFM and an LFM chirp as described in subsection 3.1.2. The LFM chirp has an instantaneous IF transition which makes it *discontinuous*. The following estimators are implemented: the *Barnes*† method of Equation 2.35; the *derivative* method of Equation 2.36 with phase unwrapping; a WVD method using Equation 2.37 and 2.45; a HHT method; and a piece-wise polynomial method. These last two are described further below.

The HHT ML method is implemented using Equation 2.52 on a discrete Hilbert spectrum. The decomposed signal is computed as described in subsection 2.5.3. The discrete Hilbert spectrum is calculated by defining a TF matrix $\boldsymbol{H}_{f,t}$ with the t axis of size $\frac{T}{T_s}$, and frequency axis set to 256 giving the frequency resolution $\Delta f = \frac{f_s}{2\times(256-1)}$‡. Then each component is sorted into the corresponding time-frequency bins in the matrix additively. The HHT MLE is obtained using Equation 2.52 where $\mathcal{L}\left[\omega|\tilde{z}[n]\right]|_{\omega=2\pi f} \coloneqq \boldsymbol{H}_{f,t}$.

A second order piece-wise polynomial method is also implemented. This result in a piece-wise linear estimate of f_{IF}. The observation $\tilde{z}[n] = \tilde{z}(t)\big|_{t=nT_s}$ is divided into $T_p = T_s \times 50$ long pieces.

$$\tilde{q}_m(\tau) = \tilde{z}(t)w\big((m-1)T_p, mT_p\big), \qquad m = [1..M],\ \tau = [0, T_p] \tag{3.5}$$

where w is the selection window defined as

$$w(t_1, t_2) = u(t-t_1) - u(t-t_2), \tag{3.6}$$

and $u(t)$ is the unit step function. For each section a polynomial phase trajectory is estimated by finding the vector $\boldsymbol{a} = [a_1, a_2, .., a_P]$§ that maximizes $D(\boldsymbol{a})$ in Equation 2.57 given the observation $\tilde{z}(t)$.

$$\boldsymbol{a} = \max_{\boldsymbol{a}} D(\boldsymbol{a}) \tag{3.7}$$

*Readers are directed to [51] for further details.

†The two-point FIR method.

‡The $\frac{1}{2}$ term is due to the analysis of the real component only, which constrains the HHT codomain to $\left\{f \in \mathbb{R} | \, 0 \le f < \frac{f_s}{2}\right\}$. Note that the discrete spectrum reduces the codomain further to a discrete set.

§Which for second-order polynomials become $\boldsymbol{a} = [a_1, a_2]$.

The maximization is found through a *simulated annealing* optimization method. Interested readers are referred to [52] for details on the method. The IF estimate is obtained by substituting $\hat{a}$ into Equation 2.59. Note that as the amplitude and start phase of the signal is not of interest, $D(\boldsymbol{a})$ is maximized as opposed to the likelihood function of Equation 2.56, reducing the optimization problem by two dimensions.

3.3 Center Frequency Estimators

Two Cyclostationary estimators are assembled based on the Spectral Correlation Density. One cyclic correlation-based center frequency estimator, and one symbol rate estimator. They utilize the FAM of Equation 2.64 with a $a(\cdot)$ being a Hamming window.

The center frequency estimator utilizes the spectral correlation as a means to estimate the center frequency of CS, while rejecting WSS signals.

Let $\hat{\boldsymbol{S}}_{f,\alpha}$ be the discrete estimate of the SCD using Equation 2.64 with cycle-frequency, and frequency resolution given by Equation 2.65 and Equation 2.67 respectively. First, the cyclic axis is reduced through a "cyclic filter", a dot-product with a window.

$$\hat{\boldsymbol{q}} = \boldsymbol{w}_\alpha \cdot \left|\hat{\boldsymbol{S}}\right| \tag{3.8}$$

The result of this "filtering" is an estimate of a frequency distribution of cyclic correlation for $\tilde{s}(t)$ in the cycle-frequencies selected by the window $\boldsymbol{w}$. The window $\boldsymbol{w}$ is a weighting function which enables the utilization of *a priori* information on the cyclic distribution of $\tilde{s}(t)$. With *a priori* knowledge on the cyclic density, a weighting function can be created using Equation 2.21. One example is shown in Figure 3.1. Here a Probability Density Function (PDF) is build from a GMM using Equation 2.21. 12 Gaussians are placed at the multiples of the true symbol rate of the signals. The Gaussians have increasing variance with harmonics to represent the uncertainties of the *true* symbol rate. Any cyclic pattern can be utilized, here the symbol-rate is used as it appears as the strongest pattern, and it is agnostic to the chirp modulation technique. The GMM parameters for the weighting function are

$$\phi_i = \left|\frac{1}{i}\right|, \tag{3.9}$$

$$\mu_i = i \times f_{symbol}\,[\text{Hz}], \tag{3.10}$$

$$\sigma_i = i \times 5\,[\text{Hz}], \tag{3.11}$$

where $i = [-6, -5, \ldots, -2, -1, 1, 2, \ldots, 5, 6]$.

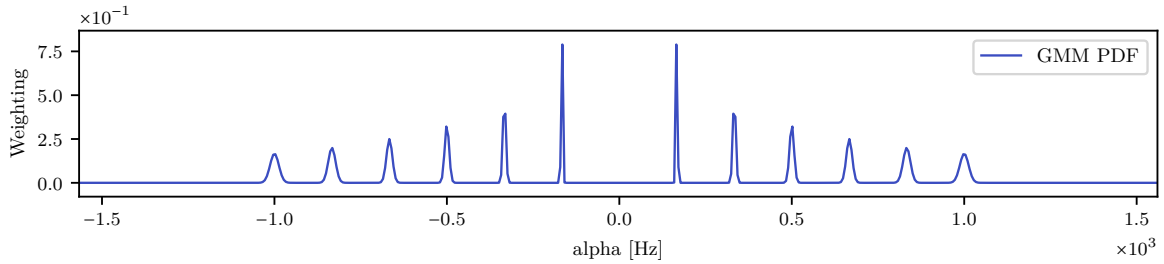

Figure 3.1: Cyclic Weighting Function

Next, the smoothed distribution is filtered with a second window $\boldsymbol{w}_f$ to capture the correlation over a frequency band. In the *a priori* case, $\boldsymbol{w}_f$ is the target cyclic correlation frequency distribution (weighted

by the initial filtering).

$$\boldsymbol{q}' = \boldsymbol{w}_f \circledast \boldsymbol{z} \tag{3.12}$$

Each frequency bin has a non-zero bandwidth given by Equation 2.76, and a null-to-null distance given by Equation 2.65. Setting $\boldsymbol{w}_\alpha = \delta[n - n_0]$[¶] and $\boldsymbol{w}_f = \delta$ then $\boldsymbol{q}'$ is reduced to an N' point PSD estimate [53] of $\tilde{z}(t)$(see Equation 2.67). The result of this processing is a distribution of correlation at selected cycle-frequencies as a function of frequency. The estimate of the center frequency is found through MLE on this distribution, using quadratic interpolation as explained in subsection 2.4.1. The estimator is implemented with various levels of prior knowledge. The variations are listed in Table 3.1

The CS based estimators are compared against a quadratic interpolation MLE method using Equation 2.24 and 2.28. The magnitude spectrum is estimated using the root of the Welch's PSD estimate of size N' with zero overlapping and a *Hann*[‖] data selection window.

Table 3.1: Center Frequency Estimator Configurations

Estimator	ω_α	$\boldsymbol{\omega}_f$
DFT MLE	N/A	N/A
CS MLE *a priori* T_s	Equation 3.9-3.11 into 2.21	Estimated 2 dB power BW
CS MLE *a priori* T_s, Ω	Equation 3.9-3.11 into 2.21	Triangle window of length $f_{max} - f_{min}$

3.4 Symbol Rate Estimation

The symbol rate estimate utilizes the estimated SCD $\hat{\boldsymbol{S}}_{f,\alpha}$ of the observation $\tilde{z}(t)$. In order to capture the cyclic correlation in the full bandwidth while rejecting out-of-band noise, a weighted average window $\boldsymbol{w}_f$ is applied along the frequency axis of $\hat{\boldsymbol{S}}_{f,\alpha}$.

$$\boldsymbol{s}_\alpha = \boldsymbol{w}_f \cdot \left|\hat{\boldsymbol{S}}^T\right| \tag{3.13}$$

The resulting vector is the cyclic autocorrelation in the frequency range given by $\boldsymbol{w}_f$. The vector has the α-range $\left[-\frac{L}{2}\Delta\alpha, -\left(\frac{L}{2}-1\right)\Delta\alpha, \ldots, \left(\frac{L}{2}-1\right)\Delta\alpha\right]$. In this thesis a rectangular window is used ($\boldsymbol{w}_\alpha = \mathbb{1}$) in the frequency range $\left[f_c - \frac{BW_{2\,\mathrm{dB}}}{2}, f_c + \frac{BW_{2\,\mathrm{dB}}}{2}\right]$ (in the non *a priori* case). Knowing the frequency distribution of the spectral correlation, a matched window can be used. Generating the window function requires an estimate of the center frequency, and the 2 dB bandwidth of the signal. These parameters have to be estimated or known *a priori*. In this thesis the bandwidth is estimated using Equation 2.29 through 2.31. The cyclic correlation in negative and positive frequency are added to obtain a single-sided correlation vector like that of Equation 2.70, in the frequency domain.

$$\hat{\boldsymbol{s}}'_\alpha = \hat{s}_\alpha[-k\Delta\alpha] + \hat{s}_\alpha[k\Delta\alpha], \qquad k = \left[-\frac{L}{2}, -\frac{L}{2}+1, \ldots, \frac{L}{2}-1\right] \tag{3.14}$$

The symbol rate is then estimated using the fundamental frequency method of Equation 2.71 replacing $\mathrm{R}_{\tilde{z}\tilde{z}}$ with $\hat{\boldsymbol{s}}'_\alpha$, and with $P = 5$ (utilizing 5 harmonic frequencies).

This estimator estimates the cycle-frequency with the highest harmonic correlation. Essentially it is a *harmonic cycle-frequency* estimator. It is applied to symbol-rate estimation through the assumption that the greatest *harmonic cycle-frequency* will come from the symbol rate[**].

[¶] n_0 is the item for which $\alpha = 0$.

[‖] Hann or sometimes called "Hanning" is a window function. Interested readers are referred to [50], [54].

[**] Correlation between identical symbols with non-identical symbol between, leading to a harmonic-like behavior in the cycle-frequency domain.

This CS estimator is implemented with various levels of prior knowledge. The prior knowledge is utilized by handing the estimator either the *true* center frequency, and/or a window $\boldsymbol{w}_f$. In addition to the frequency selective CS estimators, a full bandwidth (BW) estimator is implemented utilizing the cyclic correlation thorough the whole frequency range $\left[-\frac{f_s}{2}, \frac{f_s}{2} - \Delta f\right]$. The configurations are listed in Table 3.2.

This CS methods are compared to an autocorrelation-based method using Equation 2.71 where $\hat{f}_{symb} = \frac{1}{\hat{p}}$ and $P = 16$.

Table 3.2: Symbol Rate Estimator Configuration

Estimator	**Center Frequency**	$\boldsymbol{\omega}_f$
Autocorrelation	N/A	N/A
CS MLE	Estimated	Estimated 2 dB power BW ($\mathbb{1}$)
CS MLE full BW	N/A	Full BW $\mathbb{1}$
CS MLE *a priori* f_c	known	Estimated 2 dB power BW ($\mathbb{1}$)
CS MLE *a priori* f_c, Ω	known	Triangle window of length $f_{max} - f_{min}$

Chapter 4

Results

In this chapter, the characteristics of the proposed and implemented chirp signals are presented. Then the statistical performance of the estimators are presented, along with single-estimate, and intermediate results, highlighting the strengths and weaknesses of some estimators.

4.1 Signal Generation

As the signals are meant for communications, their cross and autocorrelation are important factors. The autocorrelation $\mathrm{R}_{\tilde{z}\tilde{z}}$ of an NLFM chirp compared to that of an equivalent LFM chirp is displayed in Figure 4.1. Both signals have equal start and stop frequency, constant envelope, and period T. The NLFM chirp has a *Hamming* $W(\cdot)$ function applied (in Equation 2.10). Note the steep side lobe taper of the NLFM chirp next to the center peak. As a consequence, it has a somewhat wider main lobe. Both signals levels at approximately same level of $-56\,\mathrm{dB}$. For approximately $|t| > 3$, the NLFM signal has the highest correlation*.

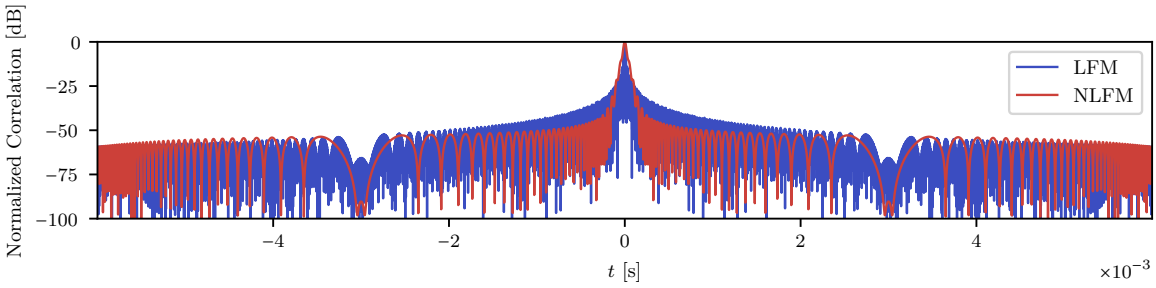

Figure 4.1: Double Sided Autocorrelation Comparison

Figure 4.2 shows the dot-product matrix for a linear chirp alphabet. The matrix shows the products in deci-Bell†, normalized to the self-dot-product. The main diagonal line of the matrix represents the self dot-product or "autocorrelation". The rest of the entries are $\boldsymbol{s}_m \cdot \boldsymbol{s}_n$ products. The ratio between the "self dot product" and cross dot product is hereby denoted as the "isolation" between symbols. The symbols in Equation 4.1 have approximately $5 - 6\,\mathrm{dB}$ isolation.

*Which is unfavourable.
†In a power scale $10\log_{10}\cdot$.

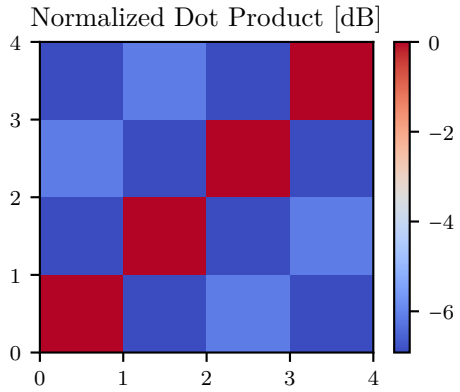

$$\boldsymbol{D} = \begin{bmatrix} 0.0 & -6.9 & -6.2 & -6.9 \\ -6.9 & 0.0 & -6.9 & -6.2 \\ -6.2 & -6.9 & 0.0 & -6.9 \\ -6.9 & -6.2 & -6.9 & 0.0 \end{bmatrix} [\text{dB}] \tag{4.1}$$

Figure 4.2: Symbol Alphabet Dot Product Matrix

The cross-correlation between the two NLFM symbols are shown in Figure 4.3. Notice how the isolation is $> 3\,\text{dB}$ greater than the discontinuous LFM symbols above at $t = 0$. The isolation is still a fair bit lower than the sidelobes of the autocorrelation displayed in Figure 4.1.

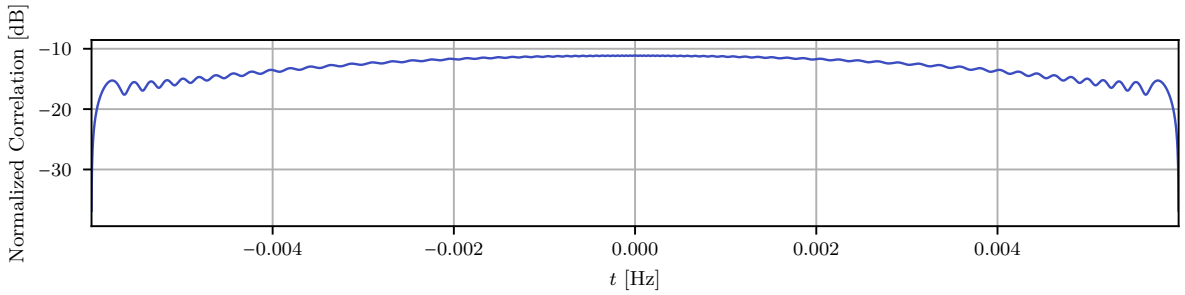

Figure 4.3: NLFM Symbols Double Sided Cross Correlation

The frequency domain power distributions of the M-ary modulated discontinuous LFM and the binary continuous NLFM are displayed in Figure 4.4 and 4.5 respectively. The PSDs are estimated using Welch's method in order to smooth the distributions. Note how the modulated LFM PSD is similar to the pure LFM of Figure 2.3, but has peaks that occur periodically across most of the frequency range. Note how the maxima of the PSD is at the outer edges of the flat top of the LFM PSD, approximately at $50\,k\text{Hz}$.

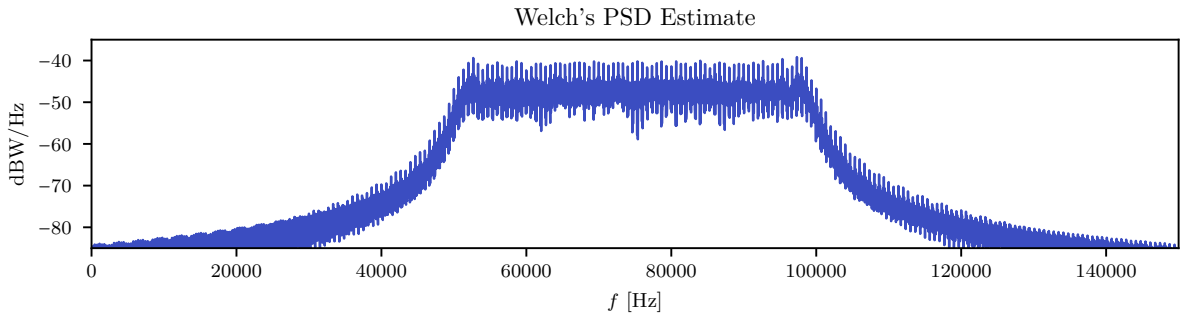

Figure 4.4: PSD of M-ary Modulated LFM Packet

The modulated NLFM PSD has apparent non-symmetric bumps along the "roof" of the PSD, in the range $[50, 100]\,[k\text{Hz}]$. Note the two power peaks adjacent to the *true* center frequency of $75\,k$Hz, and how the power drops off at the center.

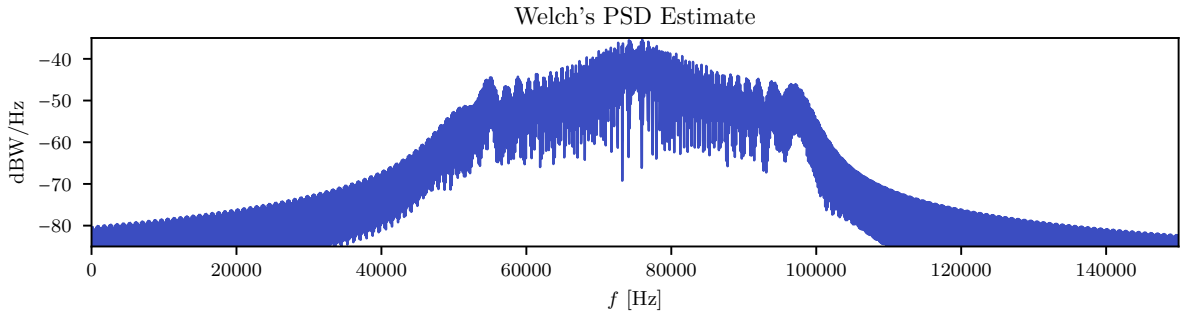

Figure 4.5: PSD of Binary Modulated NLFM Packet

4.2 Estimation of Instantaneous Frequency

4.2.1 Estimation on Continuous Non-Linear Chirps

Figure 4.6 displays the results of the IF estimator comparison when applied continuous NLFM chirps. The error measure is the *vector* or accumulated MAE[‡]. From Figure 4.6 it is apparent that there are two patterns for estimation error, one group of estimators (*direct* methods) with poor performance in low SNR, but with no apparent bound on the accuracy at high SNR, and the *indirect* methods, which outperforms the direct methods in low SNR, but have a performance bound.

The *direct* methods, the *derivative* and *Barnes Two-point FIR*, have continuously decreasing accuracy with E_b/N_0, but obtain high accuracy at high E_b/N_0 with no apparent accuracy bound. Of the two, the *derivative* method is superior and can operate at $\approx 1\,$dB lower E_b/N_0 with similar accuracy as Barnes method.

The *indirect* methods, the piece-wise polynomial, and the WVD MLE have superior accuracy to the methods above from low E_b/N_0 and up to $66 - 74\,$dB and $> 80\,$dB where the direct methods surpass the piece-wise polynomial and WVD MLE bounds respectively. These two estimators have an apparent performance bound. Among the two estimators, the piece-wise polynomial estimator operates in lower E_b/N_0 with improved accuracy compared to the WVD method, although it only has about a single dB greater operating range. The WVD has a substantially greater accuracy at its bound (it settles at a lower error level). Lastly there is the HHT MLE which in a sense is *indirect* as it first decomposes the signal, then estimates on the discrete spectrum. However, it performs only slightly better than the derivative method in the range $[33, 52]\,$dB E_b/N_0.

Figure 4.6 show that the piece-wise polynomial estimator is outperformed by the WVD estimator except for in the low E_b/N_0 unlike what's reported in [36]. In that paper however, a non-piece-wise method is considered.

[‡]The accumulated MAE is the sum of the error at each time instance (which there are $6\,\text{ms} \times 802\,000\,\text{samples/s}=4812$). An MAE of 10^6 is equivalent to a $208\,$Hz error per time instance.

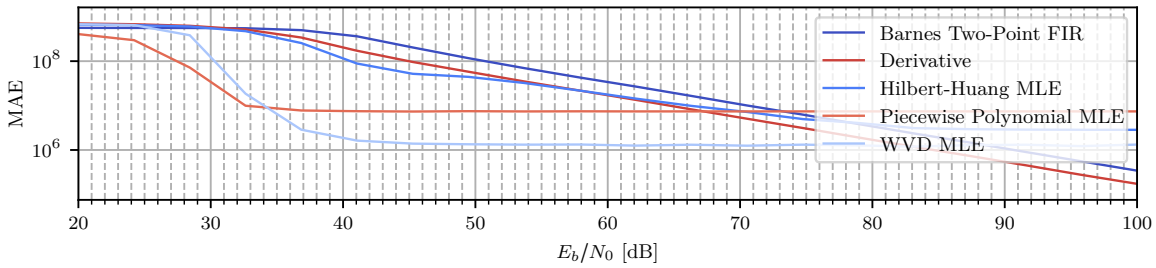

Figure 4.6: IF Estimator Performance Comparison with NLFM Observation

Figure 4.7 shows the estimated IF with its absolute error throughout the period T, for the piece-wise polynomial estimator. The signal is embedded in 10 dB of noise. The error curve in 4.7 have a sequences of ramps which converges towards a flat level at the center of the chirp, where the chirp rate is lower. It seems that even though a second-order polynomial is fitted, the result for each piece is closer to a first order fit. This is a consequence of the convergence of the minimization process of the estimator. The comparison above is thus not true to the theoretical performance of the estimator.

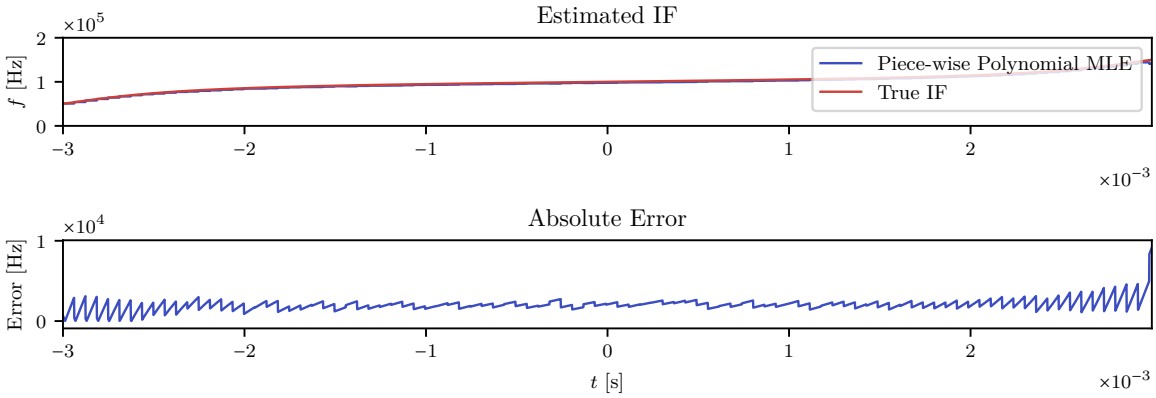

Figure 4.7: Piece-wise Polynomial IF Estimate $\frac{S}{N} = 10\,\text{dB}$

4.2.2 Estimation on Discontinuous Linear Chirps

Figure 4.8 displays an estimate of a discontinuous LFM symbol as specified in section 3.1, using the WVD MLE method. Note the large error in the range $t = [-2, 0]\,[ms]$. In this time range, the cross-terms are more dominant than the actual signal. Note the switching pattern at the beginning and end of the cross-term dominated area.

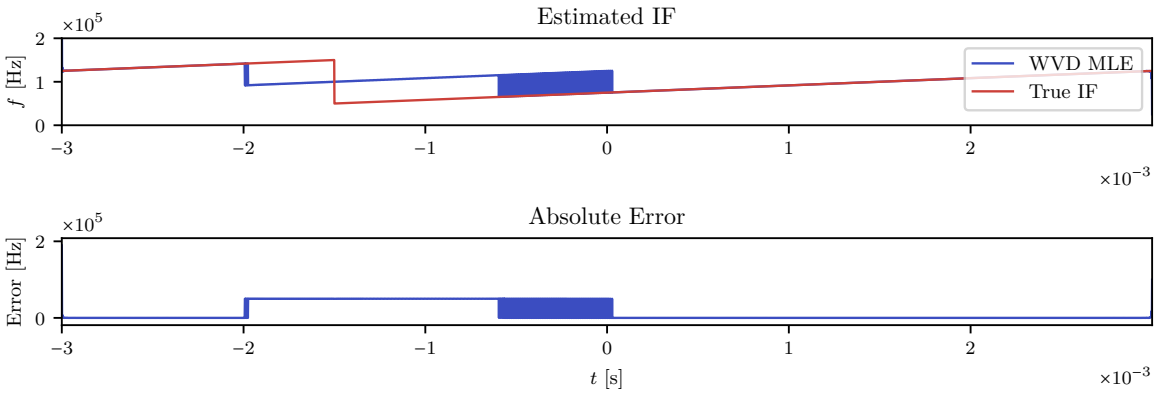

Figure 4.8: WVD MLE IF Estimate of LFM symbol with $\frac{S}{N}$ = 10 dB

Studying the results for the HHT ML estimator with the same signal (Figure 4.9), it is apparent that this estimator, while having generally more noise, manages to capture the IF transition. Notice how the estimate variance is greater for higher frequencies.

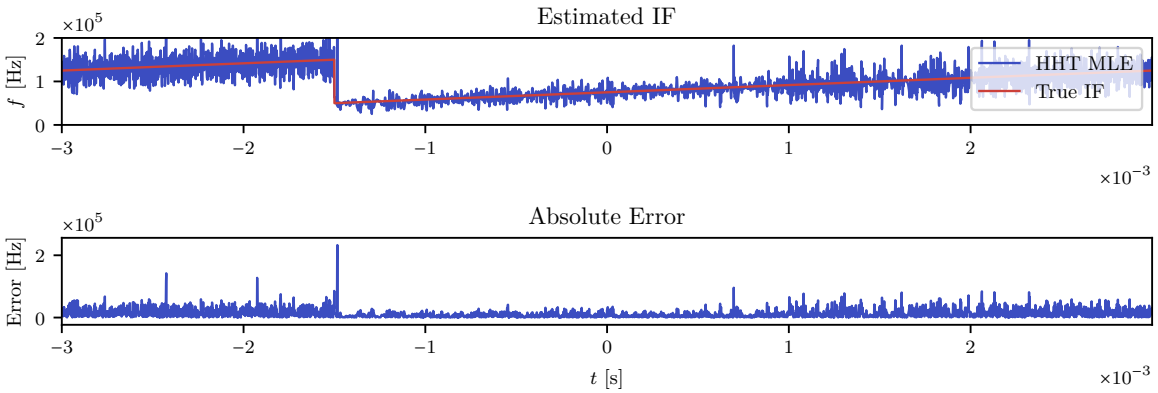

Figure 4.9: HHT MLE IF Estimate of LFM symbol with $\frac{S}{N}$ = 10 dB

Taking another look at the piece-wise polynomial method in Figure 4.10 it is apparent that this estimator has little reduction in accuracy in the *discontinuous* case. The piece estimate in the transition time of $-1.5\,ms$ has some increased error.

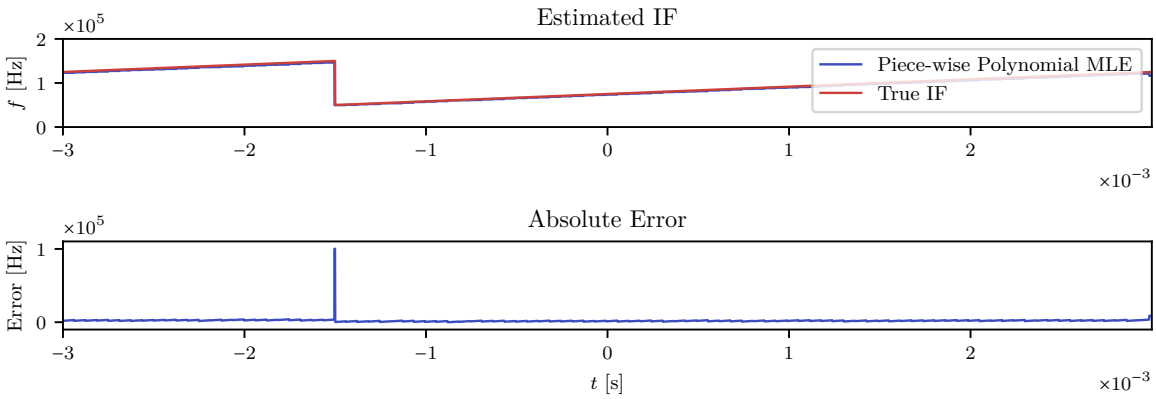

Figure 4.10: Piece-wise Polynomial IF Estimate of LFM symbol with $\frac{S}{N} = 10\,\text{dB}$

Figure 4.11 shows the performance of all estimators when observing the *discontinuous* LFM signal of the same length and bandwidth as the NLFM case (displayed in Figure 4.6). Note how the WVD has a substantially greater error rate than the HHT and polynomial methods. The polynomial method obtains the greatest accuracy of the estimators. The HHT method breaks off at approximately 40 dB, while the polynomial method continues to operate down to 28 dB E_b/N_0.

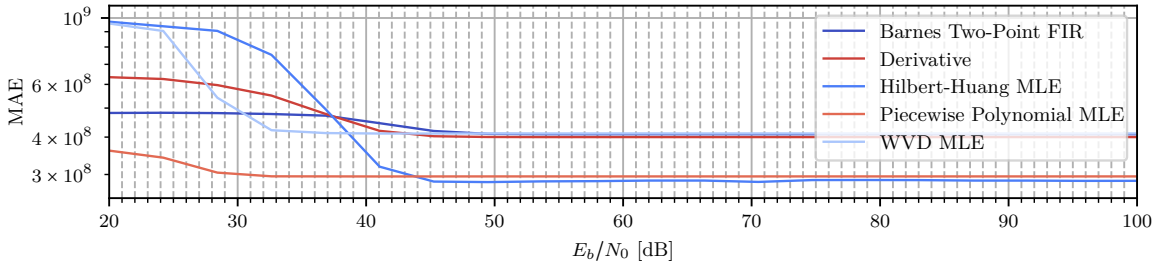

Figure 4.11: IF Estimator Performance Comparison with non-linear LFM Observation

The average runtime of the estimators over 12×41 = 492 iterations is listed in the Table 4.1. The *derivative* and *Barnes* estimators are in the sub-millisecond range. The HHT method is in the sub-second range, WVD in the order of seconds, and the *polynomial* estimator is in the order of a hundred seconds. Of the five estimators, three is time-deterministic. The polynomial method depends on an optimization approach for which the convergence rate may vary, and the HHT MLE method depends on the number of IMFs it decomposes before reaching the stopping criterion.

Table 4.1: Estimator Mean Run Time

Estimator	**Mean Run Time**
Derivative	$6.6 \times 10^{-4}\,\text{s}$
Barnes Two-Point FIR	$2.4 \times 10^{-4}\,\text{s}$
WVD MLE	$7.2\,\text{s}$
Hilbert-Huang Transform MLE	$0.647\,\text{s}$
Piece-wise Polynomial MLE	$1.1 \times 10^{2}\,\text{s}$

4.3 Cyclic Estimation of Center frequency

Figure 4.12 displays the performance of the center frequency estimators when applied NLFM modulated packets. The center frequency is estimated 1000 times per E_b/N_0 level (for each estimator). The CS estimators are compared to the classical MLE method. All three estimators seem to have an upper accuracy bound at different levels and with different convergence rates. The DFT-based estimator converges to the lowest error at < 200 Hz MAE. The CS estimator utilizing *a priori* knowledge of the symbol rate settles at the highest error level at ≈ 300 Hz MAE. However it outperforms the DFT estimator below 23 dB E_b/N_0. The CS estimator utilizing both *a priori* symbol rate information and chirp bandwidth Ω outperforms the DFT estimator below 30 dB E_b/N_0 and settles quite close at the break-off at 40 dB E_b/N_0. It has increasing error until it breaks off at 12 dB E_b/N_0, about 1 dB lower than the other two estimators.

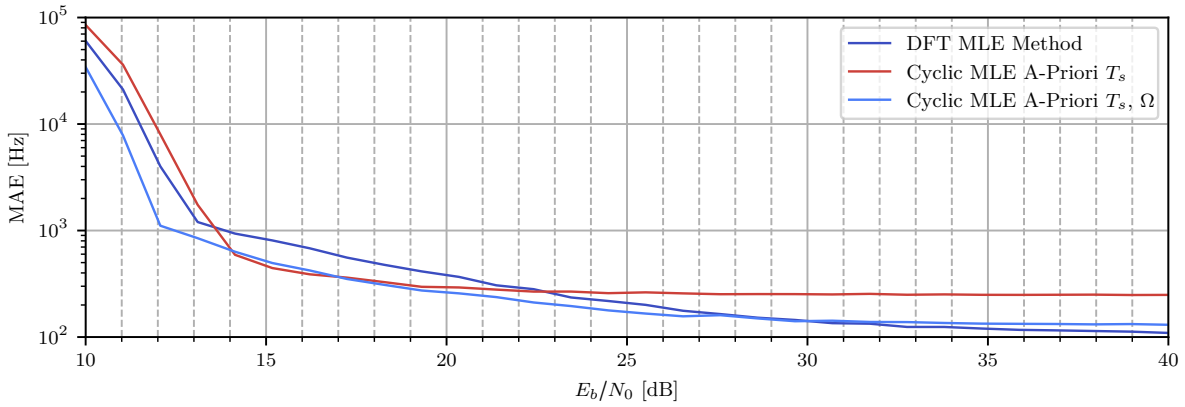

Figure 4.12: f_c Estimation

4.4 Cyclic Estimation of Symbol Rate

4.4.1 Estimation on Binary Non-Linear Chirps

This sub-section presents the performance of the symbol rate estimators when applied packets of random binary modulated NLFM pulses. Figure 4.13 displays the distribution of correlation as a function of cycle-frequency for a chirp with frequency range $[75, 125]\,[k\text{Hz}]$, symbol rate of $f_{symb} = \frac{1}{6\,\text{ms}}$ and a center frequency of $f_c = 100\,\text{kHz}$. The correlation at the chirp center frequency is displayed. Note the repeating peaks in positive and negative cycle-frequency. The major peaks are spaced approximately one symbol rate f_{symb} apart.

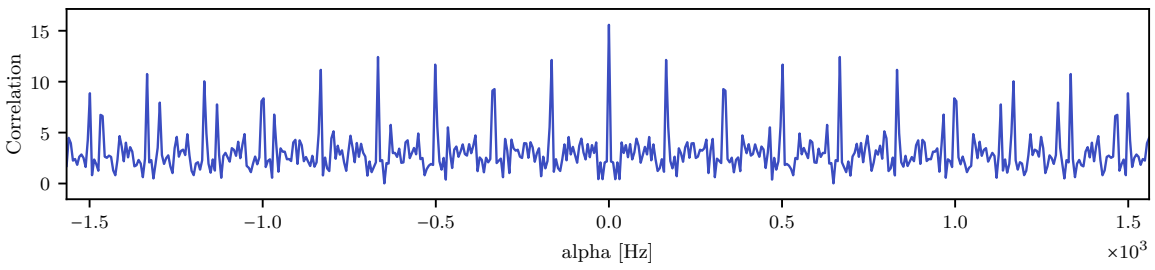

Figure 4.13: Spectral Correlogram $\left|\hat{S}_{\tilde{s}\tilde{s}^*}(\alpha, f)\right|\Big|_{f=f_c}$

The frequency distributions of the correlation for the signal in Figure 2.18 at harmonic cycle-frequencies are displayed in Figure 4.14. Most of the correlation is located in the chirp range of $[75, 125]\,[k\text{Hz}]$, but some leakage can be seen on either side of the range. Note how the frequency distribution varies with cycle-frequency.

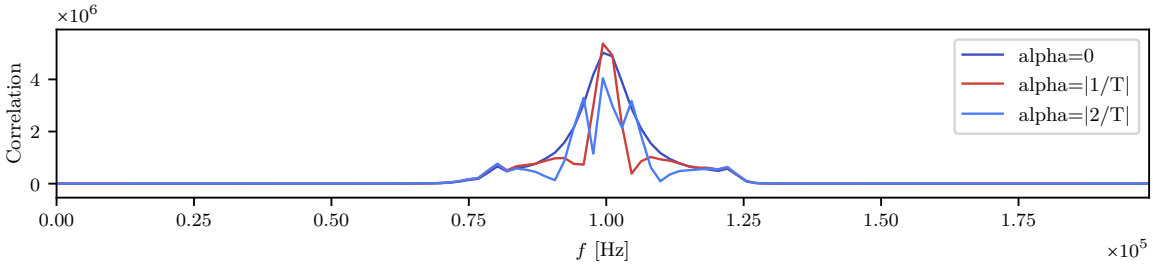

Figure 4.14: Cyclic Periodogram $\left|\hat{S}_{\tilde{s}\tilde{s}^*}(\alpha, f)\right|\Big|_{|\alpha|=nf_{symb}}$, $n = \{0, 1, 2\}$

Figure 4.15 displays the harmonic correlation for the SCD of an NLFM chirp signal through the estimator of Equation 2.71. The arg max of the displayed distribution is the estimate for the symbol rate. The figure is the equivalent of Figure 2.20 but in the frequency domain. In the figure, there is one major peak, which is close to the *true* symbol rate.

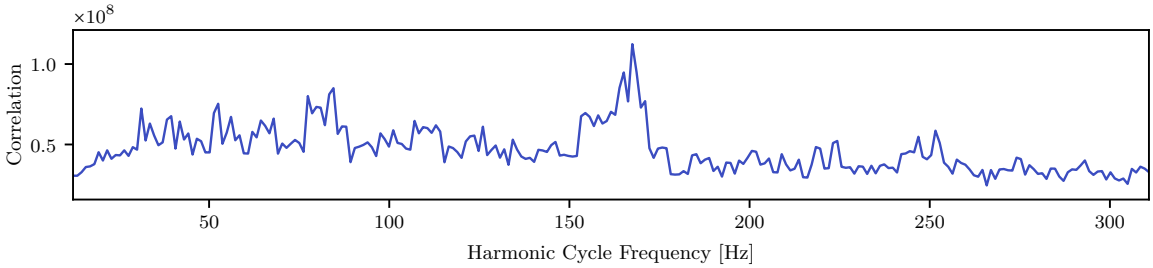

Figure 4.15: Harmonic Correlation of a 32-Bit NLFM Chirp-Per-Bit Signal

Figure 4.16 displays the performance of the symbol rate estimators when applied continuous NLFM packets. The symbol rate is estimated 100 times per E_b/N_0 level. All the estimators settles to different error levels at high E_b/N_0. The autocorrelation estimator settles to the highest error level of just under 10 Hz. All estimators breaks off between 15 and 22 dB E_b/N_0. Notice that the non-frequency selective cyclic estimator settles to the lowest error rate for $E_b/N_0 > 22$ dB. Note also how the estimators with *a priori* information dominates in the low E_b/N_0 levels below 21 dB E_b/N_0. The *Cyclic MLE A Priory* f_c which estimates 2 dB power bandwidth from a known center frequency, obtains neglectable reduction in settling error rate, and break-off E_b/N_0 level compared to the *Cyclic ML Estimator* which estimates the 2 dB power bandwidth and f_c.

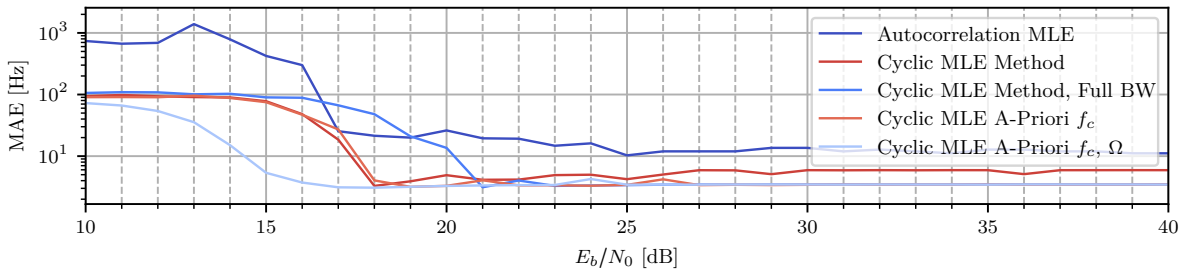

Figure 4.16: Symbol Rate Estimation Error

4.4.2 Estimation on M-ary Discontinuous Linear Chirps

This sub-section presents the performance of the estimators when applied packets of random M-ary modulated LFM chirps with the shifting scheme specified in Equation 3.2. The signals are of the same length and bandwidth Ω as the ones in the previous sub-section. Figure 4.17 displays the SCD for a packet. Note how the spectral correlation is evenly spread out through the chirp range of $[75, 125]\,[k\text{Hz}]$. There is strong correlation at cycle-frequencies $\alpha = nf_{symb}$, $n \in \mathbb{Z}$. The strongest correlation is located at $\alpha \approx \pm 4 \times f_{symb}$.

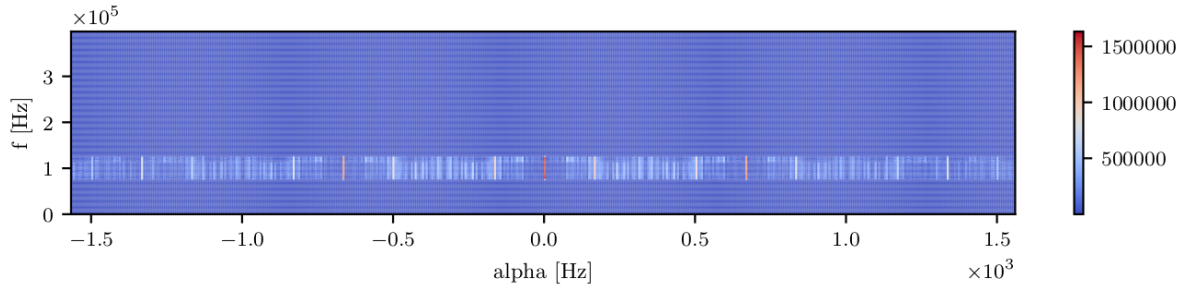

Figure 4.17: Spectral Correlation Density Estimate $\left|\hat{S}_{\tilde{s}\tilde{s}^*}(\alpha, f)\right|$ of a 32-symbol M-ary LFM Packet (Positive Frequencies Only)

Figure 4.18 displays the correlation from Figure 4.17 along the cycle-frequency axis at the chirp center frequency. Note how the peak at $\alpha = 0$ is substantially lower than in the NLFM case. Note also how the correlation peaks are less distinct compared to that of the NLFM case.

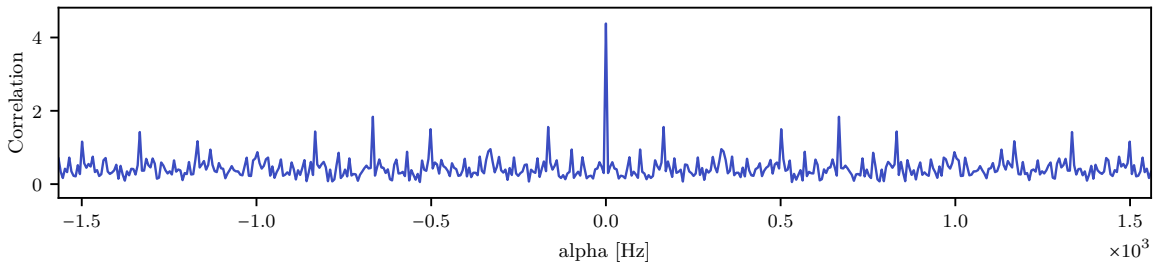

Figure 4.18: Spectral Correlogram $\left|\hat{S}_{\tilde{s}\tilde{s}^*}(\alpha, f)\right|_{f=f_c}$

The frequency distributions of the correlation for the signal in Figure 4.17 at harmonic cycle-frequencies

are displayed in Figure 4.19. The correlation is evenly spread out in the chirp frequency range for multiple harmonics of f_{symb}, unlike the NLFM case. Note how the fourth harmonic has slightly greater magnitude than the fundamental in red.

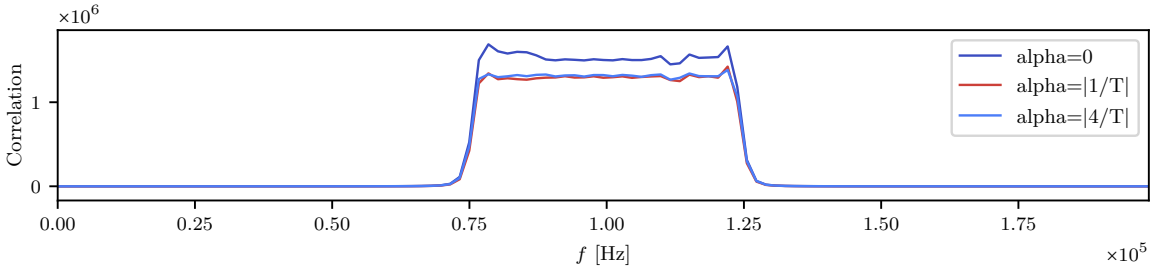

Figure 4.19: Cyclic Periodogram $\left|\hat{S}_{\tilde{s}\tilde{s}^*}(\alpha, f)\right|\Big|_{|\alpha|=nf_{symb}}$, $n = \{0, 1, 4\}$

Figure 4.20 presents the performance of the estimators when applied signals with a random symbol sequence. The symbol rate is estimated 1000 times per E_b/N_0 level. The CS estimators settle at an error rate of almost an order greater than in the NLFM case. Additionally, the various CS estimators settle at the same error rate. The benchmark autocorrelation estimator has substantially greater error than the cyclic estimators.

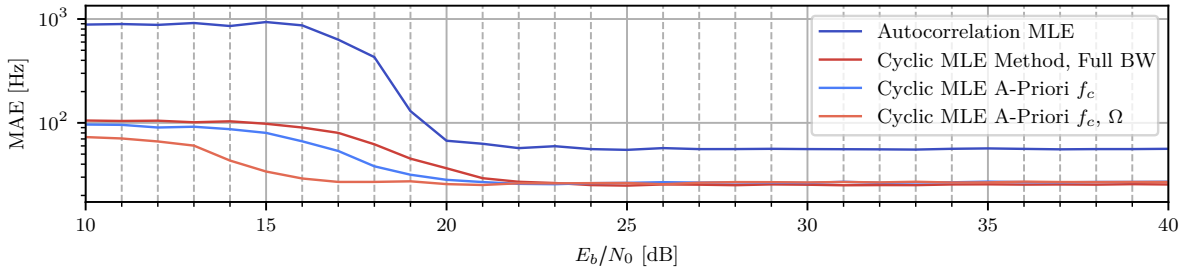

Figure 4.20: Symbol Rate Estimation Error, M-ary LFM

Figure 4.21 presents the performance of the estimators when applied a synchronization sequence (as specified in Equation 3.4). The symbol rate is estimated 1000 times per E_b/N_0 level. Note how all estimators have close to an order of magnitude lower error bounds than in the case above. Here, the autocorrelation-based estimator performs superiorly, and obtains almost an additional order of magnitude greater accuracy than the CS estimators. All of the estimators break of at approximately the same E_b/N_0, but as can be seen in both Figure 4.20 and 4.21; The estimators with *a priori* center frequency and chirp bandwidth can operate at close to 3-5 dB lower E_b/N_0 than the others.

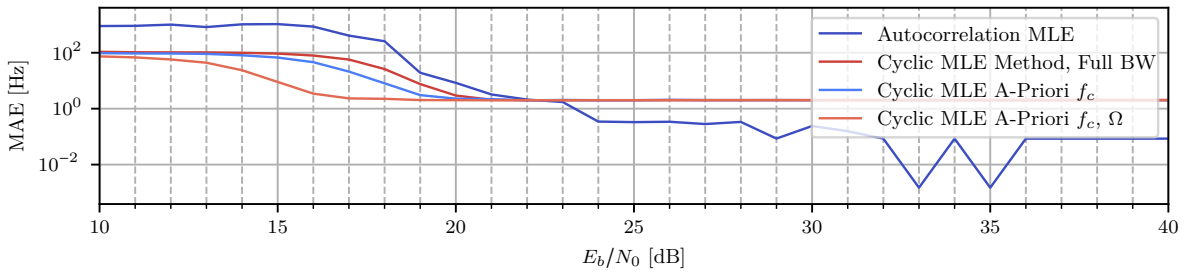

Figure 4.21: Symbol Rate Estimation Error, M-ary LFM with sync sequence

The mean run times of the estimators are displayed in Table 4.2. Note that the autocorrelation method is an order of magnitude slower than the CS estimators.

Table 4.2: Symbol Rate Estimator Mean Run Time

Estimator	**Mean Run Time**
Autocorrelation MLE	4.4 s
Cyclic MLE Method	0.22 s
Cyclic MLE Method, Full BW	0.26 s
Cyclic MLE A Priori f_c	0.25 s
Cyclic MLE A Priori f_c, Ω	0.23 s

Chapter 5

Discussion

In this chapter, the implemented methods and their experimental results are discussed. Apparent strengths and weaknesses of the various estimators are discussed with extrapolation to their real-world implications. Lastly, there are some comments on the generated signals.

5.1 Signal Analysis

5.1.1 IF Estimation

It is apparent that Barnes and the derivative method although fast, are quite inaccurate in any practical E_b/N_0 range, compared to the WVD and the piece-wise polynomial method. Interestingly, the derivative method performs superior to the Barnes method in practically the whole E_b/N_0 range. This is the opposite of the behavior pointed out by Barnes [26]. In this thesis however, a *phase unwrapping* is applied to resolve the ambiguities which are pointed out by Barnes. The Barnes method does run faster than the derivative method, which might justify its use in time-critical applications.

The WVD estimator obtains the lowest error rate in the practical E_b/N_0 regions for NLFM chirps. This is the opposite of what is stated in the literature [27], [36]. This could be a result of a low chirp rate $\gamma(t)$ leading to low levels of cross terms. In a real-world scenario, there would be multi-path terms which would distort the signal, reducing its performance greatly. There are polynomial WVD methods which improves the estimate for NLFM waveforms [45], but these assume a *continuous* IF. With discontinuous chirp communication gaining popularity, such constraints seem impractical. The weakness of the WVD is apparent for estimates on discontinuous chirps. For these signals the performance breaks down to a level where it might not be practical for classification purposes.

The piece-wise polynomial method seems to be a good intermediate between the pure WVD MLE and polynomial WVD methods. As the polynomial method is free of "cross-terms" and as observed in the results, the piece-wise nature allows relatively drastic IF jumps (discontinuities). It performs worse than the WVD MLE method in the continuous case, but outperforms all estimators in the discontinuous case. From Figure 4.7 it is obvious that there exist better solutions to the optimization problems, as it seems like all pieces have resulted in a first-order solution*. The *true* error rate of this estimator remains to be seen. The piece-wise estimation partially removes the need for prior information on the (equivalent)† polynomial order of the observation. For observations of high (equivalent) polynomial order $P \in \mathbb{N}$, the piece separation reduces the problem from $\mathbb{R}^P$ to $M \times \mathbb{R}^2$, where M is the number of pieces to estimate. Yet with this problem size reduction, the piece-wise polynomial estimator still runs orders of magnitude slower than the others. It is of course possible that an inefficient optimization algorithm

*This is observed when maximizing for higher-order polynomials as well.
†As the observation might be linear or piece-wise linear.

is used, in addition to a high number of samples to solve for. The piece-wise computing as well as the optimization approach are exceptionally parallelizable. Each piece can be computed independently, and the optimization can be parallelized even further. It might reach practical speeds when optimized on a GPU[‡] or FPGA[§].

The HHT ML estimator performs only marginally better than the derivative method. This is perhaps not too surprising considering that the IF of each IMF is estimated using that exact method. In the discontinuous LFM case, it outperforms most estimators and seem to be a suitable TF transform in moderate SNR scenarios. Estimators using the Hilbert spectrum can reject interfering signal components if they are weaker than the target signal. Domínguez et al. proposes the use of instantaneous envelope (magnitude as a function of time) for classification, this parameter could be directly extracted together with the IF from the spectrum [47].

The IF vector of a chirp contains a lot of information, and as such, requires a high E_b/N_0 to accurately estimate the frequency path (compared to the other estimators). Perhaps the IF could be reduced to a smaller set of parameters that optimally would be linearly separable between chirps with different IF trajectories. Examples of such parameters could be: the upper and lower frequency of the chirp; the location of the power maxima, which for asymmetrical IF-paths can be anywhere between the upper and lower frequency; a parameter representing the rate of which the IF changes (mean chirp rate $\langle\gamma(t)\rangle_T$). For symmetrical chirps, an additional parameter could be the first-order polynomial fit of the phase path, (e.g. using Equation 3.7). The problem with these reduced parameters is that they typically require assumptions to be made, e.g. continuous IF, symmetrical IF path, etc. Thus the methods lose their generality. As described in section 2.1; The IF path of the chirp is closely related to its PSD. Some IF-related parameters could thus be extracted from its PSD, or the frequency distribution of the cycle-frequencies of a SCD. This would allow multiple overlapping signals to be characterized independently[¶]. Examples of such parameters could be the skewness, kurtosis, and symmetry (like proposed by Dominguez [47]) of the frequency distribution, either using the PSD or specific cycle-frequencies.

The IF estimators are intended to estimate on a single chirp. Communication signals contain many such chirps (assuming a chirp-per-symbol scheme). These estimators thus rely on the quality of the symbol rate estimate, to separate the chirps.

5.1.2 Center Frequency Estimation

Figure 4.4 and 4.5 display the fundamental issues with estimating the center frequency on signals with a non-zero bandwidth. As the center frequency is not located at the maxima of the PSD, the DFT ML method cannot find the *true* center frequency. The center frequency could be found if the PSD is filtered with a matched filter, but this requires full knowledge for the signal (apart from the center frequency) which is unrealistic to assume. A complex exponential has an infinitesimally narrow bandwidth; Therefore, as the DFT size increases so does the estimate accuracy. However, for finite bandwidth signals there exists an optimal DFT size, where the frequency response of the DFT bins are the closest to the matched filter of the observation. This also applies to the FAM-based CS estimators, as its channelization is performed using a STFT (see Equation 2.64 and 2.66). With a great DFT size and high SNR, both the DFT and the CS-based estimators would be biased, as the frequency domain peaks are located adjacent to the *true* center frequency. From figures 4.14 and 4.19 it is apparent that the CS estimator won't be as biased for the particular NLFM case, as the LFM case.

Based on the results, it is apparent that of the considered *a priori* cases, knowledge on the chirp bandwidth Ω seems to be the most powerful. This prior knowledge could easily be applied to improve the simpler DFT ML estimator.

[‡]A Graphics Processing Unit (GPU) is an Integrated Circuit (IC) which can compute problems using multiple cores for a single function.

[§]A Field-Programmable Gate Array (FPGA) is a specialized IC which can be configured for parallel, and real-time processing.

[¶]This with the assumption that the overlapping signals have different dominant cycle-frequencies.

Duda [22] proposes that windowing along with polynomial interpolation of the periodogram improves frequency estimates. In the case of a single chirp with an asymmetric IF trajectory, the windows will skew the periodogram which would lead to biased estimators. The windowed methods seem not appropriate for single chirp cases. However, for multi-pulse signals like those studied in this thesis, it might improve the estimates.

The results show that there is little to gain from utilizing the CS-based estimators for center frequency estimation, even with *a priori* information. However, utilizing filters in the cyclic axis allows the separation of simultaneous signals. That is, by applying filters which only measure the correlation at cycle-frequencies which are harmonics of symbol rate, then the signals can be separated. This would not be possible with the magnitude spectrum.

In this thesis, only "symmetrical" chirps are used. For asymmetrical chirps, that is, chirps for which the mean of the PSD is not at the chirp frequency midpoint $f_{stop} - \frac{f_{stop}-f_{start}}{2}$, the center frequency definition must be explicitly defined. It could be defined as the mean of the PSD, the frequency midpoint as defined above, etc. As this parameter is estimated for classification purposes, crude center frequency estimators might be sufficient.

5.1.3 Symbol Rate Estimation

The CS class of estimators obtains greater accuracy at a lower computational cost than the traditional autocorrelation counterpart, except for the LFM-with-synchronization scenario. This latter scenario seems more realistic with regards to having a synchronization sequence. All of the estimators performed worse in the M-ary case than in the binary. This might be a consequence of fewer repetitions of symbols. This repetition is the root of the cyclic properties. An interesting result from the LFM case, is how the strongest correlation appears at cycle-frequency $\alpha = 4f_{symb}$. This might be a result of how the symbols are created by shifting the chirp by $\frac{1}{M}T$, which makes a symbol correlate with the shifted version at cycle-frequency $\alpha = Mf_{symb}$, similar to what is observed. If this is true, then the order of the modulation could be found through CS analysis, for shifted modulation schemes like LoRa.

The chirp bandwidth is shown to improve the estimates the most, of the studied *a priori* parameters. It enables several dB increase in the practical operative E_b/N_0 range. The *a priori* f_c estimator with estimated 2 dB power bandwidth gains only 2 dB of operative range over the full BW estimator. Perhaps a better power bandwidth estimate would close some of this performance gap. The bandwidth estimator is dependent on the magnitude spectrum peak to be above the noise floor by the power reduction amount. With this particular estimator, there is an *a priori* trade-off between accuracy and SNR operating range.

5.1.4 Execution Time

The estimators are run in parallel while the computer is used for various other tasks. As a result, the time estimates have some inaccuracies. The estimators are written in Python, where some estimators utilize greater degrees of low-level optimizations than others. The code is written with libraries such as *NumPy* and *SciPy* [55], which utilize efficient codes written in FORTRAN, C and C++. Some estimators have less of such optimization, which could lead to additional inaccuracies. The execution time estimates indicate the order of magnitude which can be expected on single-core operation.

5.2 Signal Generation

Most chirp-based communication systems utilize linear chirp schemes. The implemented NLFM signaling scheme is thus not very representative of what one can expect to see on the spectrum (at least for communication purposes). They do however open up for substantially lower inter-symbol isolation (cross-correlation between symbols) as displayed in Figure 4.3, which makes these suitable for robust low-power communications and MIMO schemes. The optimization method required to create the IF path makes it impractical to solve for new IF trajectories in real time. This means that the path must be stored in the

transmitter devices. The steep IF trajectories obtainable in with NLFM chirps increases the required sample rate of the transmit-receive systems (in order to avoid aliasing).

The LFM modulated scheme has lower inter-symbol isolation than the NLFM symbols. The waveforms are however simple to generate and easy to manage. With an increasing number of symbols, the time shift of each symbol reduces, which leads to a reduction in inter-symbol isolation. This signaling scheme seems like it would be limited to a low number of symbols before the inter-symbol isolation is too low.

5.3 Further Work

The best-performing IF estimator in this thesis is the piece-wise polynomial phase trajectory estimator. It however runs orders of magnitude slower than its counterparts when run on a single core. A computationally efficient implementation should be studied, in order to conclude whether the precise method is applicable in real-time classification systems. Variations like the faster piece-wise polynomial *least squares* method should be compared to the ML method.

The WVD shows great promise on continuous chirp signals, but breaks down on discontinuous. Methods such as the PWD and refined methods such as Choi-Williams Distribution (CWD)[‖] should be studied further.

The presented estimators and results show that there are methods to extract the center frequency, IF and symbol rate of arbitrary chirp waveforms. One question that remains is whether the chosen parameters with the obtainable accuracy is enough to separate different chirp signals. Further experiments with classification networks should be performed in order to quantify the effectiveness of the estimators.

[‖]Choi and Williams proposes a method of reducing these cross terms in what has later been termed the CWD function [56]. Both the CWD and the WVD are special cases of Cohens class of Time-Frequency distributions [31].

Chapter 6

Conclusion

In this thesis, a set of estimators are assembled in an attempt to create an algorithm that can characterize chirp modulated signals. A method of generating non-linear chirps through a chirp-rate forming method is implemented. It shows promise, but requires a computationally costly optimization approach. A second LoRa-like signal generator is proposed and implemented. Those signals obtain lower isolation between the symbols than the NLFM counterpart.

A set of IF estimators are implemented and tested against two sets of challenging chirp pulses. Of the estimators, the polynomial phase ML estimator shows superior operating SNR range, and beat the others by several dBs in both the continuous non-linear case and the discontinuous linear case. It suffers from high computing requirements, but is exceptionally parallelizable. The WVD ML estimator is shown to work great for continuous IF signals, but breaks down for discontinuous. An HHT ML method is proposed as a solution, which is relatively fast, and is decent in both the continuous and discontinuous cases. All of the estimators requires substantially greater SNR than the two other studied parameters.

A cycle-frequency-based center frequency estimator is implemented utilizing knowledge of the symbol rate. The estimator is compared against a traditional magnitude spectrum ML method. The cycle-frequency-based estimator outperforms the traditional estimator in low SNR, and with *a-priori* knowledge on chirp bandwidth and symbol rate, it manages to obtain approximately the same accuracy for high SNR. As such the cycle-frequency based method is a candidate for parameter estimaton on simultaneous and overlapping signals.

Lastly a proposed harmonic cycle-frequency estimator is implemented and used as a symbol rate estimator. It obtains estimates within Hertz to tens of Hertz of the true value. It outperforms a harmonic autocorrelation based estimator in two out of three test scenarios. The cycle-frequency approach is shown to run an order of magnitude faster than the autocorrelation approach.

Bibliography

[1] A. Hazza, M. Shoaib, S. A. Alshebeili, and A. Fahad, "An overview of feature-based methods for digital modulation classification," in *2013 1st International Conference on Communications, Signal Processing, and their Applications (ICCSPA)*, 2013, pp. 1–6.

[2] A. Kawalec and R. Owczarek, "Specific emitter identification using intrapulse data," in *First European Radar Conference, 2004. EURAD.*, 2004, pp. 249–252.

[3] C. M. Spooner, "Multi-resolution white-space detection for cognitive radio," in *MILCOM 2007 - IEEE Military Communications Conference*, 2007, pp. 1–9.

[4] W. S. J. L. Xu and M. Zhou, "Likelihood-ratio approaches to automatic modulation classification," *IEEE Transactions on Systems, Man, and Cybernetics, Part C (Applications and Reviews)*, vol. 41, no. 4, pp. 455–469, 2011.

[5] B. A. Bash, D. Goeckel, D. Towsley, and S. Guha, "Hiding information in noise: Fundamental limits of covert wireless communication," *IEEE Communications Magazine*, vol. 53, no. 12, pp. 26–31, Dec. 2015.

[6] P. G. Cook and W. Bonser, "Architectural overview of the speakeasy system," *IEEE Journal on Selected Areas in Communications*, vol. 17, no. 4, pp. 650–661, 1999.

[7] H. Shen, W. Zhang, X. An, and K. Kwak, "Ds-pam uwb system using non-linear chirp waveform," *Etri Journal - ETRI J*, vol. 29, pp. 322–328, Jun. 2007.

[8] L. L. Gutman and G. E. Prescott, "System quality factors for lpi communications," *IEEE Aerospace and Electronic Systems Magazine*, vol. 4, no. 12, pp. 25–28, Dec. 1989.

[9] G. Madzarov and D. Gjorgjevikj, "Multi-class classification using support vector machines in decision tree architecture," in *IEEE EUROCON 2009*, May 2009, pp. 288–295.

[10] A. Swami and B. M. Sadler, "Hierarchical digital modulation classification using cumulants," *IEEE Transactions on Communications*, vol. 48, no. 3, pp. 416–429, 2000.

[11] C. M. Spooner and A. N. Mody, "Wideband cyclostationary signal processing using sparse subsets of narrowband subchannels," *IEEE Transactions on Cognitive Communications and Networking*, vol. 4, no. 2, pp. 162–176, 2018.

[12] Doerry and A. Doerry, "Generating nonlinear fm chirp waveforms for radar," Sep. 2006.

[13] C. Gao, K. C. Teh, A. Liu, and H. Sun, "Piecewise lfm waveform for mimo radar," *IEEE Transactions on Aerospace and Electronic Systems*, vol. 52, no. 2, pp. 590–602, Apr. 2016.

[14] B. C. Levy, *Principles of Signal Detection and Parameter Estimation*, 1st ed. Springer Publishing Company, Incorporated, 2008.

[15] G. Kalivas, *Digital Radio System Design*. Wiley Publishing, 2010.

[16] G. Ferré and A. Giremus, "Lora physical layer principle and performance analysis," in *2018 25th IEEE International Conference on Electronics, Circuits and Systems (ICECS)*, 2018, pp. 65–68.

[17] O. Bernard, A. Seller, and N. Sornin, "Low power long range transmitter," Patent EP2763321A1, Feb. 2013.

[18] C. Bernier, F. Dehmas, and N. Deparis, "Low complexity lora frame synchronization for ultra-low power software-defined radios," *IEEE Transactions on Communications*, pp. 1–1, 2020.

[19] I. Goodfellow, Y. Bengio, and A. Courville, *Deep Learning*. The MIT Press, 2016.

[20] P. Stoica, R. L. Moses, B. Friedlander, and T. Soderstrom, "Maximum likelihood estimation of the parameters of multiple sinusoids from noisy measurements," *IEEE Transactions on Acoustics, Speech, and Signal Processing*, vol. 37, no. 3, pp. 378–392, Mar. 1989.

[21] J. W. Cooley and J. W. Tukey, "An Algorithm for the Machine Calculation of Complex Fourier Series," *Math. Comput.*, vol. 19, pp. 297–301, 1965.

[22] K. Duda, "Dft interpolation algorithm for kaiser-bessel and dolph-chebyshev windows," *IEEE Transactions on Instrumentation and Measurement*, vol. 60, no. 3, pp. 784–790, 2011.

[23] K. Werner and F. Germain, "Sinusoidal parameter estimation using quadratic interpolation around power-scaled magnitude spectrum peaks," *Applied Sciences*, vol. 6, no. 10, p. 306, Oct. 2016.

[24] E. Jacobsen and P. Kootsookos, "Fast, accurate frequency estimators [dsp tips tricks]," *IEEE Signal Processing Magazine*, vol. 24, no. 3, pp. 123–125, 2007.

[25] C. M. McIntyre and D. A. Dermott, "A new fine-frequency estimation algorithm based on parabolic regression," in *[Proceedings] ICASSP-92: 1992 IEEE International Conference on Acoustics, Speech, and Signal Processing*, vol. 2, 1992, 541–544 vol.2.

[26] A. E. Barnes, "The calculation of instantaneous frequency and instantaneous bandwidth," *GEOPHYSICS*, vol. 57, no. 11, pp. 1520–1524, 1992.

[27] K. M. Wong and Q. Jin, "Estimation of the time-varying frequency of a signal: The cramer-rao bound and the application of wigner distribution," *IEEE Transactions on Acoustics, Speech, and Signal Processing*, vol. 38, no. 3, pp. 519–536, 1990.

[28] N. Huang, Z. Shen, S. Long, M. Wu, H. Shih, Q. Zheng, N. Yen, C.-C. Tung, and H. Liu, "The empirical mode decomposition and the hilbert spectrum for nonlinear and non-stationary time series analysis," *Proceedings of the Royal Society of London. Series A: Mathematical, Physical and Engineering Sciences*, vol. 454, pp. 903–995, Mar. 1998.

[29] K. Abratkiewicz and P. Samczyski, "A block method using the chirp rate estimation for nlfm radar pulse reconstruction," *Sensors*, vol. 19, no. 22, 2019.

[30] E. Sejdic, I. Djurovic, and L. Stankovic, "Quantitative performance analysis of scalogram as instantaneous frequency estimator," *IEEE Transactions on Signal Processing*, vol. 56, no. 8, pp. 3837–3845, 2008.

[31] L. Cohen, *Time-Frequency Analysis: Theory and Applications*. USA: Prentice-Hall, Inc., 1995.

[32] P. Pace, *Detecting and Classifying Low Probability of Intercept Radar*, ser. Artech House radar library. Artech House, 2009.

[33] M. Sun, C. C. Li, L. N. Sekhar, and R. J. Sclabassi, "A wigner spectral analyzer for nonstationary signals," *IEEE Transactions on Instrumentation and Measurement*, vol. 38, no. 5, pp. 961–966, 1989.

[34] L. Stankovic and S. Stankovic, "On the wigner distribution of discrete-time noisy signals with application to the study of quantization effects," *IEEE Transactions on Signal Processing*, vol. 42, no. 7, pp. 1863–1867, 1994.

[35] B. Boashash and P. Black, "An efficient real-time implementation of the wigner-ville distribution," *IEEE Transactions on Acoustics, Speech, and Signal Processing*, vol. 35, no. 11, pp. 1611–1618, 1987.

[36] B. Boashash, P. O'Shea, and M. Arnold, "Algorithms for instantaneous frequency estimation: A comparative study," *Proceedings of SPIE - The International Society for Optical Engineering*, vol. 1348, Nov. 1990.

[37] R. Rato, M. Ortigueira, and A. Batista, "On the hht, its problems, and some solutions," *Mechanical Systems and Signal Processing*, vol. 22, no. 6, pp. 1374–1394, 2008, Special Issue: Mechatronics.

[38] G. Rilling, P. Flandrin, P. Goncalves, and J. M. Lilly, "Bivariate empirical mode decomposition," *IEEE Signal Processing Letters*, vol. 14, no. 12, pp. 936–939, 2007.

[39] G. Rilling, P. Flandrin, and P. Gonçalves, "On empirical mode decomposition and its algorithms," *Proceedings of IEEE-EURASIP Workshop on Nonlinear Signal and Image Processing NSIP-03*, vol. 3, Jun. 2003.

[40] D. C. Bowman and J. M. Lees, "The HilbertHuang Transform: A High Resolution Spectral Method for Nonlinear and Nonstationary Time Series," *Seismological Research Letters*, vol. 84, no. 6, pp. 1074–1080, Nov. 2013.
[41] J. Deshpande, *Pyhht*, `https://github.com/jaidevd/pyhht/`, 2019.
[42] J. Zhang, F. Wang, O. A. Dobre, and Z. Zhong, "Specific emitter identification via hilberthuang transform in single-hop and relaying scenarios," *IEEE Transactions on Information Forensics and Security*, vol. 11, no. 6, pp. 1192–1205, 2016.
[43] Y. Yuan, Z. Huang, H. Wu, and X. Wang, "Specific emitter identification based on hilbert-huang transform-based time-frequency-energy distribution features," *IET Communications*, vol. 8, no. 13, pp. 2404–2412, 2014.
[44] J. Sun, G. Xu, W. Ren, and Z. Yan, "Radar emitter classification based on unidimensional convolutional neural network," *IET Radar, Sonar Navigation*, vol. 12, no. 8, pp. 862–867, 2018.
[45] B. Boashash and P. O'Shea, "Polynomial wigner-ville distributions and their relationship to time-varying higher order spectra," *IEEE Transactions on Signal Processing*, vol. 42, no. 1, pp. 216–220, Jan. 1994.
[46] A. Napolitano, *Cyclostationary Processes and Time Series*, A. Napolitano, Ed. Academic Press, 2020.
[47] L. Domínguez, J. Borrallo, J. García, and B. Mezcua, "A general approach to the automatic classification of radiocommunication signals," *Signal Processing*, vol. 22, no. 3, pp. 239–250, 1991.
[48] R. S. Roberts, W. A. Brown, and H. H. Loomis, "Computationally efficient algorithms for cyclic spectral analysis," *IEEE Signal Processing Magazine*, vol. 8, no. 2, pp. 38–49, Apr. 1991.
[49] J. Wise, J. Caprio, and T. Parks, "Maximum likelihood pitch estimation," *IEEE Transactions on Acoustics, Speech, and Signal Processing*, vol. 24, no. 5, pp. 418–423, Oct. 1976.
[50] J. G. Proakis and D. K. Manolakis, *Digital Signal Processing (4th Edition)*, Fourth edition, International. Pearson, 2014.
[51] R. Byrd, P. Lu, J. Nocedal, and C. Zhu, "A limited memory algorithm for bound constrained optimization," *SIAM Journal on Scientific Computing*, vol. 16, no. 5, pp. 1190–1208, 1995.
[52] Y. Xiang, D. Sun, W. Fan, and X. Gong, "Generalized simulated annealing algorithm and its application to the thomson model," *Physics Letters A*, vol. 233, no. 3, pp. 216–220, 1997.
[53] P. Welch, "The use of fast fourier transform for the estimation of power spectra: A method based on time averaging over short, modified periodograms," *IEEE Transactions on Audio and Electroacoustics*, vol. 15, no. 2, pp. 70–73, Jun. 1967.
[54] R. B. Blackman and J. W. Tukey, "The measurement of power spectra from the point of view of communications engineering part i," *The Bell System Technical Journal*, vol. 37, no. 1, pp. 185–282, 1958.
[55] P. Virtanen, R. Gommers, T. E. Oliphant, M. Haberland, T. Reddy, D. Cournapeau, E. Burovski, P. Peterson, W. Weckesser, J. Bright, S. J. van der Walt, M. Brett, J. Wilson, K. Jarrod Millman, N. Mayorov, A. R. J. Nelson, E. Jones, R. Kern, E. Larson, C. Carey, . Polat, Y. Feng, E. W. Moore, J. Vand erPlas, D. Laxalde, J. Perktold, R. Cimrman, I. Henriksen, E. A. Quintero, C. R. Harris, A. M. Archibald, A. H. Ribeiro, F. Pedregosa, P. van Mulbregt, and S. 1. 0. Contributors, "SciPy 1.0: Fundamental Algorithms for Scientific Computing in Python," *Nature Methods*, vol. 17, pp. 261–272, 2020.
[56] H. Choi and W. J. Williams, "Improved time-frequency representation of multicomponent signals using exponential kernels," *IEEE Transactions on Acoustics, Speech, and Signal Processing*, vol. 37, no. 6, pp. 862–871, 1989.
[57] *Anaconda software distribution*, version Vers. 2-2.4.0, 2020.

Appendix A

Recreation of this Work

All signals and simulation in this thesis are built on free and open source tools. All estimators and signal generation algorithms implemented for this thesis are released in the *rf-tool* python package. The package is hosted on PyPi: `https://pypi.org/project/rf-tool/`. The source code for this package is hosted on GitHub: `https://github.com/ErikBuer/rf-tool`.

To install, open a terminal (e.g. anaconda prompt in Windows [57]) and run the following command:

```
pip install rf-tool
```

The code for running the simulations and generating the plots in this thesis is hosted on GitHub: `https://github.com/ErikBuer/ChirpAnalyzer`. To download the package, open a folder of choice and run the following command in a terminal*:

```
git clone https://github.com/ErikBuer/ChirpAnalyzer.git
```

*This requires Git to be installed.

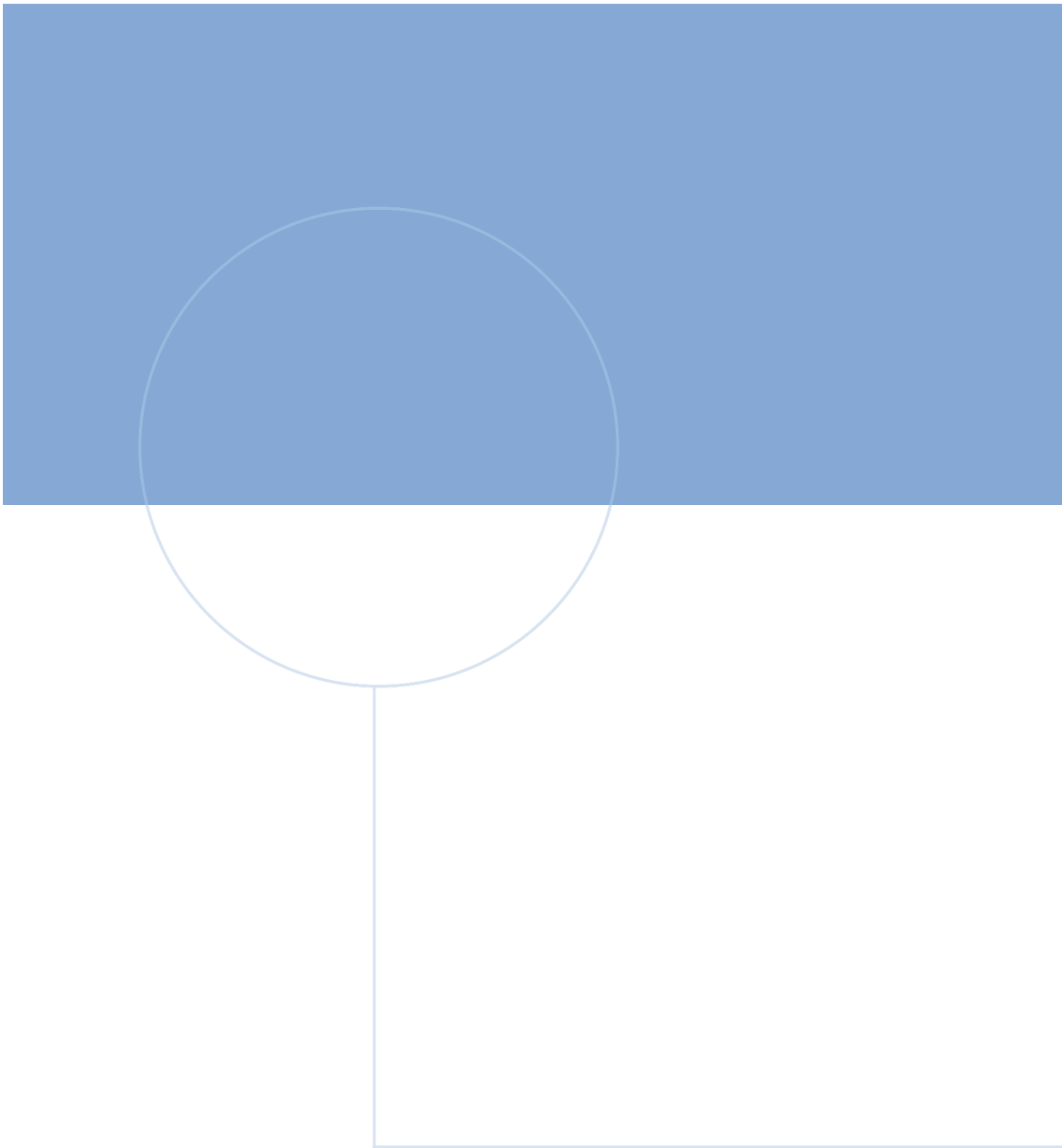

NTNU
Norwegian University of
Science and Technology

KONGSBERG